AN EXPERIMENTAL ANALYSIS OF MAGNETORHEOLOGICAL (MR) DAMPING FOR
VIBRATION MITIGATION


A thesis presented to the faculty of the Graduate School of Western Carolina University in partial
fulfillment of the requirements for the degree of Master of Science in Technology.


By

William Ralph Deaton IV


Advisor: Dr. Sudhir Kaul
Assistant Professor
Department of Engineering and Technology

Committee Members:
Dr. Wesley Stone, Engineering and Technology
Dr. Robert Adams, Engineering and Technology
June 2015

# ACKNOWLEDGEMENTS

TABLE OF CONTENTS

LIST OF TABLES

LIST OF FIGURES

ABSTRACT

AN EXPERIMENTAL ANALYSIS OF MAGNETORHEOLOGICAL (MR) DAMPING FOR

VIBRATION MITIGATION

William Ralph Deaton IV, M.S.T

Western Carolina University (June 2015)

Advisor: Dr. Sudhir Kaul


Magnetorheological (MR) dampers have emerged as a viable means of semi-active damping in multiple

industry applications. The semi-active nature of these dampers is a significant attribute since the damper

functions as a passive damper in the event of a failure. While there have been other smart materials like

ferroelectric, piezoelectric, shape memory alloys, etc. that have been successfully used, MR fluids exhibit

a unique combination of completely reversible effect, very low response time, high durability and very

low energy requirements that make them suitable for vibration control in a wide variety of applications.

This study presents results from an experimental investigation that has been carried out to evaluate the

performance of a MR damper for vibration mitigation. The capability of a commercial MR damper to

isolate a payload from base excitation is analyzed and the damper parameters are identified to simulate

the capability of the damper with regards to transmissibility. Simulation results are presented for multiple

levels of damping exhibited by the MR damper. Multiple iterations of testing have been performed in

order to evaluate the influence of variables such as input current to the electromagnet of the damper, mass

of the payload, excitation frequency and excitation amplitude. Although temperature is known to be a

significant parameter that influences the performance of the MR damper, it has not been critical for the

purposes of this study. This can be primarily attributed to the small displacement amplitudes that have

been used for excitation. Results indicate that the MR damper is successful in mitigating vibrations

transmitted to the payload. Vibration mitigation is quantified by comparing the root mean square (RMS)

of the time history of acceleration of the base with that of the payload. Peak values of acceleration are

also compared. Displacement transmissibility results directly demonstrate the variable damping capability of the MR damper. Although the stiffness constant of the damper may also change, it is not seen to vary appreciably in this study since the excitation amplitude is limited to a low threshold. The damper is found to be robust with an inherent ability of handling payload and excitation variability. It is observed that increasing the input current to the electromagnet around the MR fluid directly results in an increase in damping, therefore, making the use of these dampers viable in applications where payloads and excitation inputs are expected to change during operation. These features of robustness and controllability make the use of MR dampers very attractive in a large range of applications.

CHAPTER 1 :  INTRODUCTION


Active materials are being increasingly investigated to overcome constraints associated with

material selection. Magnetorheological (MR) fluid is one such active material that can offer a range of

damping properties instead of one fixed damping value, as is common with passive dampers. However,

the challenge in using MR dampers is that they exhibit highly nonlinear attributes such as hysteresis,

saturation, etc. Furthermore, direct control of damping characteristics of MR dampers is difficult since

damping levels are governed by the strength of the magnetic field, velocity input, displacement amplitude

as well as operating and fluid temperatures. There is a significant amount of existing literature that

investigates different aspects of usage and control of MR fluids [1 – 3].

MR dampers have been used and investigated for two decades. However, they have not been as

commonly used as traditional dampers, shock absorbers, spring-damper systems, or rubber dampers.

Some comparisons have been drawn between the effectiveness of passive dampers and active damping,

and to identify the pros and cons associated with the use of a smart material such as MR fluid for

damping. Though there is a large body of work in the existing literature on the use and application of MR

dampers, the use of these dampers is still not widespread. The robustness of these dampers in the presence

of variables such as damper current, excitation amplitude, excitation frequency, etc. is still being actively

investigated for various applications. This study focuses on evaluating the performance of a commercial

MR damper in order to comprehend its capability in the presence of multiple variables, with the input

from the shaker table as the primary source of excitation. The study involves an experimental

determination of the variable damping capability of the MR damper, and identification of its semi-active

damping over a range of excitation levels. The aim of this study is to develop a holistic understanding of

the capabilities of the damper, and identify its limitations for vibration mitigation. This thesis seeks to

answer the following questions:

1. What is the influence of variables such as excitation amplitude, excitation frequency, damper current, and payload on vibration mitigation capabilities of a MR damper in the presence of base excitation?

2. How do the damping and stiffness properties of the MR damper change? How do these changing properties influence vibration mitigation?

## 1.1.    Scope of Thesis

This thesis examines the capability of a commercially available MR damper through experimental analysis. The damper is tested on the tensile tester to identify its varying stiffness and damping characteristics. These characteristics are used to develop a preliminary mathematical model to compute expected acceleration transmissibility and force transmissibility for a single degree-of-freedom model.

Subsequently, the damper is used to perform testing on the shaker table in the presence of varying excitation frequency, varying excitation amplitude, varying payload and changing input current of the electromagnet of the damper. All the variables are changed within the technical capabilities of the damper as well as the capabilities of the equipment in the laboratory. The acceleration data is captured through accelerometers and then collected through a data acquisition system. The data is subsequently post-processed and analyzed in MATLAB®.

It may be noted that this thesis does not aim to determine the optimum settings or conditions for the damper. This is primarily because the optimum settings will largely depend on the specific application that the damper is being used for. Also, this thesis does not develop a control algorithm or program to continuously vary the damping levels. The control algorithm would also significantly depend on the application for which the damper is being used. The primary contribution of this research is in answering the research questions identified in the previous section, and in outlining an elaborate experimental procedure that can be used repeatedly to test a MR damper for vibration mitigation.

## 1.2.    Overview of Thesis

This section provides an overview of the entire document. In Chapter 1, a brief introduction is provided along with the research questions and a chapter-by-chapter overview. Chapter 2 discusses the

relevant background and the existing literature associated with this study. Literature on semi-active control and active materials is also briefly discussed in this chapter.

Chapter 3 discusses the mathematical model that has been developed to simulate a single degree-of-freedom system that is subject to base excitation. The parameters identified from tensile testing of the MR damper are used for the model. Overall results of expected acceleration and force transmissibility with varying damping levels are also presented in this chapter.

Chapter 4 presents all the details associated with the development of the experimental setup. The experimental results are discussed and analyzed in detail. Chapter 5 summarizes the main findings and the main results of this study. Trends observed with multiple test parameters are also discussed in this chapter. The future scope of research for this study is also discussed in this chapter.

## 1.3. Key Terms

Following is a list of some of the key terminology that is relevant to this thesis and will be used throughout the document:

Rheology – The study of the flow and deformation of matter.

Magnetorheological fluid (MR fluid) – A fluid whose viscosity and flow characteristics can be altered with the application of a magnetic field [4].

Hysteresis – This is a property associated with the time dependence of a parameter. It is exhibited by many dynamic systems.

Damper – A device designed to mitigate the transfer of forces from one object to another connected object. A damper can be passive, semi-active or active.

Shaker table – An electro-dynamic testing device that can generate a wide range of frequencies and amplitudes of vibration.

Shaker Base (Base) – The top plate of the shaker table that can be used as the test table.

Payload – The load connected to the damper that is excited through the shaker table.

CHAPTER 2 :   LITERATURE REVIEW

Researchers have been studying various means of minimizing the forces transmitted from one structural member to another for a very long time, particularly for applications where vibrations can cause damage or fatigue over a period of time. This chapter lists some recent research from the existing literature that is relevant to the content of this study. This chapter also provides the pertinent background information that is not covered in Chapter 1. A brief discussion is provided on the findings from some of the research that has been reviewed during the course of this study.

## 2.1.    Magnetorheological Fluid

Magnetorheological (MR) fluid belongs to a group of materials classified as "smart materials" due to their ability to change their properties in response to an external stimulus [4]. MR fluids change their rheological (fluid or plastic flow) properties through the application of an external magnetic field. There are multiple means of using this fluid in applications such as MR elastomers, MR fluids, and MR foams. Usage of MR fluid in a damper is pretty common and is the focus of this study.

MR fluid is a dense suspension of magnetized particles dispersed within a supporting liquid medium, usually oil or silicone-based. The magnetized particles in the fluid are typically $10^{-7}$ to $10^{-5}$ meters in diameter [4]. Without the influence of a magnetic field, the particles are uniformly distributed within the supporting medium, behaving as a viscous fluid. Upon application of a magnetic field, the particles re-orient themselves into alignment of the field, providing a structural rigidity to the fluid. Up to a limit, an increase in the strength of the magnetic field directly increases the effective viscosity of the fluid. This transition is completely reversible and can be achieved in milliseconds [1, 4]. An illustration of MR fluid structure, with and without a magnetic field, can be seen in Figure 2.1. It may be noted that another material called as the Electro-Rheological (ER) fluid exhibits similar properties. ER fluids exhibit properties that are similar to MR fluids with a similar makeup of particles of significantly small size that are suspended in an oil-based medium, but the primary difference is in the mode of activation – an electrical field as opposed to a magnetic field. Despite the similarities between ER and MR fluids, a

significant drawback to extensive usage of ER fluids is their requirement of a very high electrical field, often approaching 5kV/mm. In comparison, an electromagnet controlling the MR fluids may require up to 12V to produce an equivalent effect [5].
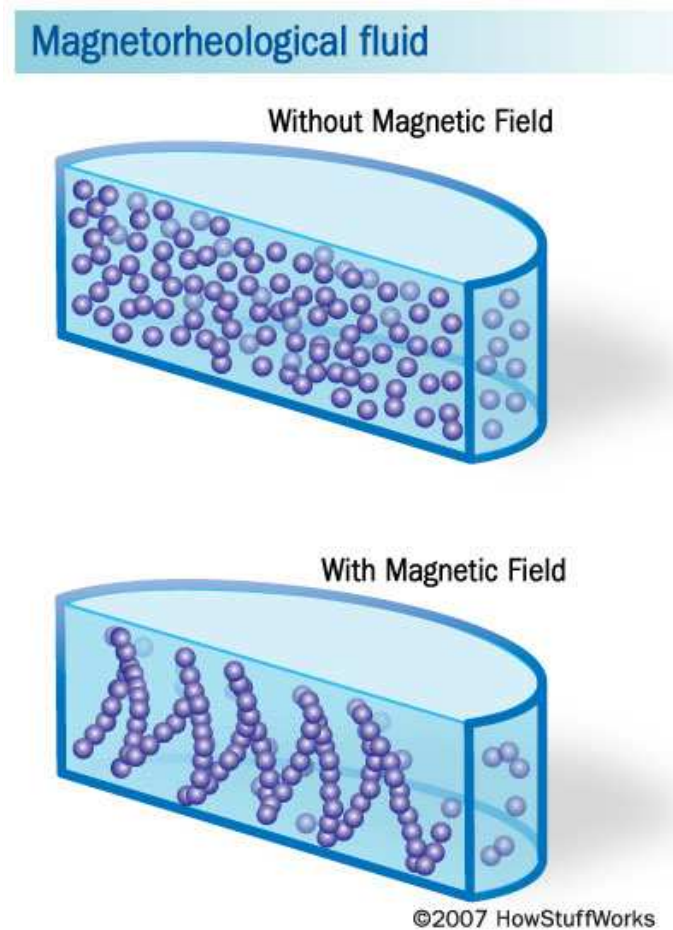


Figure 2.1: Magnetorheological fluid [6].

By varying the strength of a magnetic field within close proximity of the MR fluid, the effective yield strength of the fluid can be directly modified by using an electromagnet with a change in the input current of the electromagnet. MR fluids can be used in various operational modes. The three main modes are the valve or flow mode, the shear mode, and the squeeze mode [4]. These modes are illustrated in Figure 2.2.
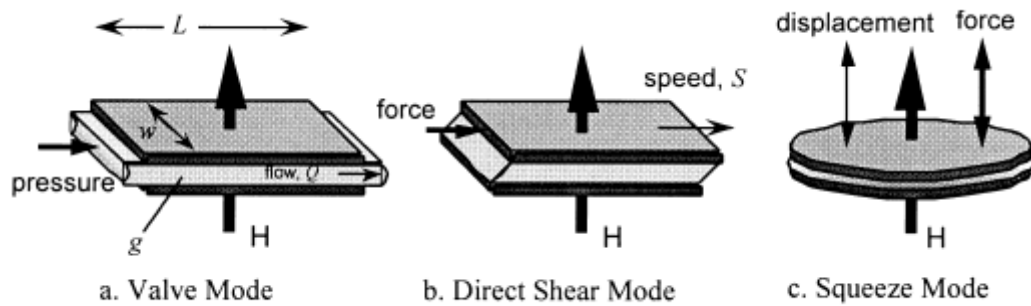
Figure 2.2: Operation modes for Magnetorheological fluids [4].

There are pros and cons to each of the three modes that have been discussed in the relevant literature along with the design and applications of the dampers using these three modes [1]. For the purposes of this study, the valve mode is of particular interest since it is commonly used in MR dampers.

## 2.2. Magnetorheological Damping

While passive dampers in the form of hydraulic dashpots have existed for a long time in various forms, dampers that exhibit an ability to vary their damping properties are relatively more recent. Although a mechanical adjustment of the size of the fluid aperture can be used to vary damping levels, these designs have severe limitations in terms of their operating range, and also exhibit a relatively long response time. MR dampers mitigate these limitations with near-infinite adjustability and a response time measuring in milliseconds. This has made the use of MR damping possible in applications that can benefit from semi-active damping.

### 2.2.1. Applications and Devices

Currently, the most well-known application of MR dampers is within the automotive sector under such trade names as "MagnaRide" that has been developed by General Motors [5]. Manufacturers of some high-end vehicles are taking advantage of the MR damper's easily-adjustable properties to provide a driver-selectable suspension setting that can overcome the tradeoff between handling and ride comfort. A passive suspension system typically involves a compromise between ride comfort and handling since the choice of the design parameters associated with these characteristics meets the needs of one at the

expense of the other. The 2016 Chevrolet Camaro is an example of a vehicle featuring the "MagnaRide" system, allowing for selection of pre-determined ride settings, such as a "Sport" or "Track" mode, with MR dampers serving as the adjustable suspension components.

### 2.2.2. Semi-active Control

MR dampers are categorized as "semi-active". This indicates that these dampers retain some of their damping properties even when there is no power supply, or even when the controller fails. In such cases the damper reverts to a passive state, working as a passive damper. This property is a significant advantage over similar systems which are not semi-active, since in the event of a power failure (or other similar failures) the MR damper can continue to function as a damper, albeit at a potentially reduced capacity. This is an advantage over fully active dampers that have significant power requirements, and lead to complete breakdown in case of a power failure or a controller failure.

The development of control algorithms for MR dampers becomes complex due to some specific characteristics exhibited by the fluids such as hysteresis and saturation. These characteristics and issues associated with shear thickening and temperature dependence of the fluid have been investigated in the existing literature [2, 3]. Furthermore, control characteristics are important since damping levels cannot be controlled directly. Damping is controlled indirectly by changing the current input to the electromagnet that in turn governs the damping levels [2]. There has also been a significant amount of research in the development of mathematical models that can be used to simulate the behavior of MR fluids. These models include high fidelity models such as the Bouc-Wen model [7] with an inherent evolutionary variable and multiple parameters that can be used to represent the hysteretic behavior. The Bouc-Wen model is accurate but computationally intensive and could be difficult to implement in an online control environment. However, this model is pretty accurate for the purposes of simulation, as demonstrated in the literature [7]. Recursive models have been used by incorporating the time history of displacement and velocity [8, 9] in order to explore possible models that can be used for control. Such models have an inherent ability to adapt to changing inputs and operating conditions, and can be used to predict the expected damping force that can in turn be used to compute control parameters. However, it has been

reported that including force feedback in the recursive model is critical and may not be practical in some applications [9]. It is pointed out in the literature that the performance of a suspension system that uses MR dampers is largely dependent on the choice of the control algorithm [10]. It is, therefore, crucial to perform elaborate testing in order to clearly determine the influence of control parameters on the capability of a suspension system that uses MR dampers.

### 2.3. Magnetorheological Damping - Vibration Mitigation

Experimental aspects of vibration mitigation have been studied with semi-active dampers that can be tuned [11] by using a paddle damper. This study is important to the research presented in this document because of some similarities in the experimental techniques. Sarigul-Klijn et all [11] created an MR damper by saturating a section of open-cell foam with commercially available MR fluid, and activated it with an electromagnet. A shaker table was used to generate vibrational forces, and accelerometers were attached to the base of the shaker as well as the payload situated on top of the damper. The acceleration of the payload was compared to the acceleration of the base in terms of hysteresis loops. These loops could be analyzed to determine the level of damping of the device. Figure 2.3 shows one such hysteresis plot from this paper.
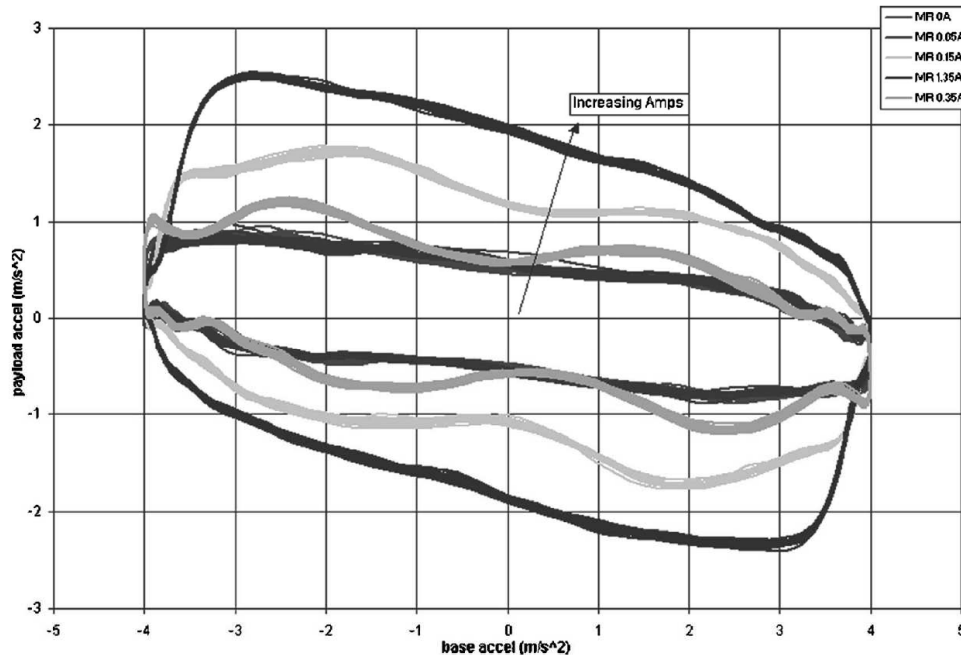
Fig. 4  Experimental acceleration hysteresis loops at 5 Hz excitation and 2 m/s² input magnitude

Figure 2.3: Acceleration hysteresis plot [11].

A quarter-car model is commonly used in the dynamic analysis of suspensions systems for automobiles. One such study includes the experimental analysis of alternative semi-active control methods [12]. This study tested three different control policies for semi-active dampers.  The study used a MR damper that was built in what is referred to as a "quarter-car" test setup. The ratio between the sprung mass and input displacement was measured and compared between the three policies. Some aspects of this study are relevant to this research since the MR damper was used in evaluating control strategies for the suspension system.

Another study on the use of a semi-active suspension system using MR fluids was tested on the road and showed a comparison between passive damping and MR damping [13]. This study replaced the passive dampers on a vehicle's suspension with MR dampers that were controlled by an algorithm that was developed specifically for the study. The test vehicle was driven over a road surface at various speeds, and the ride quality was monitored by a number of accelerometers placed throughout the vehicle. According to this study, "None of the previously published works on MR dampers deals with the

9

investigation of vehicle suspension system installed with MR dampers under the real road profile". This study has been useful for comparing the results obtained in the proposed research. Other studies have also evaluated the mechanical performance of a MR damper experimentally [14], particularly to determine the controllability of the damper with the change of current of the electromagnet.

The use of magnetorheological dampers has also been investigated for shock isolation [15] to investigate the practical aspects associated with replacing a passive shock isolation system with a semi-active shock isolation system consisting of a MR damping system. However, this study was entirely theoretical, and incorporated several control methods to assess shock isolation without any experimental validation.

The experimental setup for this research study resembles the setup used in other similar studies (e.g. [11]). This setup consists of a shaker table that provides a vibration input directly to the damper that is mounted on the shaker table. The payload is assembled to the damper and is excited through the shaker table. The transmissibility plots and the acceleration hysteresis plots resulting from this test setup of the MR damper are directly compared to passive damping settings and to the multiple settings of the damper.

## 2.4.    Conclusion

In summary, the literature study conducted for this research has been used to identify some critical parameters associated with MR fluids and MR dampers. These parameters have been useful for designing the experimental setup and for developing the test matrix for this study. Additionally, the literature study has been used to develop an understanding of MR dampers and to build an overall context for the research.

This thesis tests the robustness of a commercial MR damper in order to quantify its capability to mitigate vibrations in a controllable manner. Acceleration transmissibility is evaluated for a base shaking configuration and the influence of multiple parameters such as the input current to the electromagnet, displacement amplitude, and input frequency is evaluated. The theoretical models used for this research are discussed in Chapter 3 followed by the presentation of experimental results in Chapter 4. Chapter 5 lists the conclusions and the scope for future work.

CHAPTER 3 : DAMPING CHARACTERISTICS AND MODELING

This chapter discusses the mathematical model used to analyze displacement and force transmissibility of the damper. The results are compared to an undamped system in order to evaluate the use of active damping. The analysis results are discussed in detail.

### 3.1.    Transmissibility

The capabilities of the magnetorheological (MR) Damper used in this study can be expressed in terms of transmissibility. However, since the damper behavior can be controlled by the current input to the electromagnet, the transmissibility of this damper exhibits varying characteristics. In this study, acceleration at the excitation source has been directly measured and compared to the acceleration of the isolated mass (payload). Theoretically, these accelerations are typically expressed in terms of a ratio between the payload and the base to evaluate acceleration transmissibility.

To obtain the damper parameters, a universal testing machine has been used to load the damper under various conditions and levels of current input to the damper. This testing yielded the force-deflection and force-velocity characteristics, enabling the identification of the MR damper parameters seen in Table 3.1. This testing and test setup are discussed in detail in Chapter 4. In Table 3.1, $k_i$ is the stiffness of the MR damper; $c_i$ is the damping constant, and the damping ratio, $\zeta_i = \frac{c_i}{2\sqrt{m\,k_i}}$.

Table 3.1: Damper Parameters.

| Current (A) | $k_i$ (N/m) | $c_i$ (N-s/m) | $\zeta_i$ ($m = 11.5$ kg) | $\zeta_i$ ($m = 14.9$ kg) |
|---|---|---|---|---|
| 0 | 100 | 2.5 | 0.037 | 0.032 |
| 0.5 | 150 | 20 | 0.240 | 0.211 |
| 1 | 150 | 30 | 0.361 | 0.317 |
| 1.5 | 150 | 37.5 | 0.451 | 0.396 |

### 3.2.    Frequency Response

Looking at the difference in the frequency response between the base and payload, transmissibility of vibrations can be directly compared. The frequency response charts that were created

in this study show the differences in the frequency response of the base (input) and payload (output). The data that was collected during testing was in time domain and has been transformed into frequency domain by applying the Fast Fourier transform, and noise has been removed by using a Butterworth filter. The transformed is then plotted to compare the base and payload signals. One such example of a frequency response chart is shown in Figure 3.1, generated from the experimental data. All the plots for the test configurations will be discussed in detail in Chapter 4.
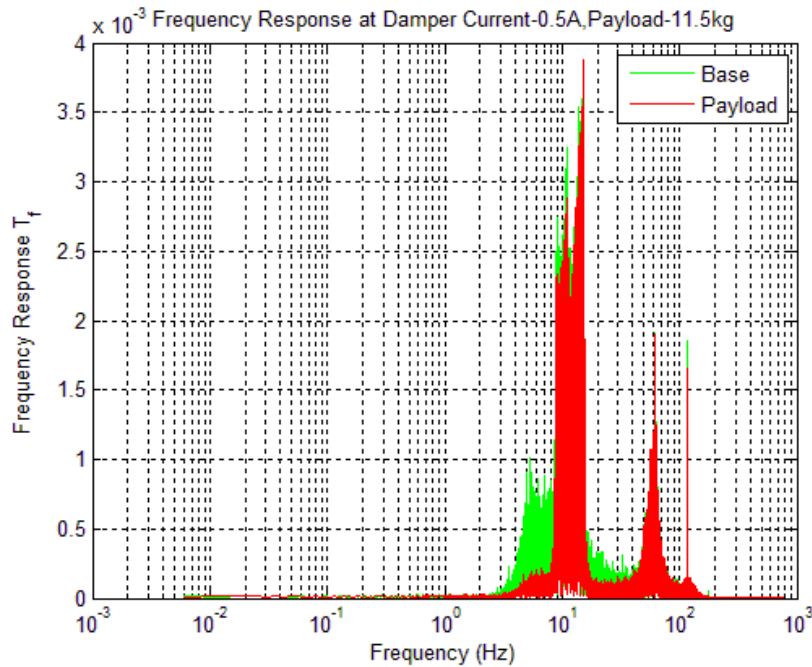


Figure 3.1: Frequency response plot, logarithmic scale; payload of 11.5 kg, damper current of 0.5A, frequency sweep from 9-16 Hz, amplitude of 400 mVpp.

### 3.3.    Modeling

To create a mathematical model to examine transmissibility and frequency response, a simplified spring-mass-damper model has been used. This is a single degree of freedom system with a lumped mass that is excited at the base, as seen in Figure 3.2 below.
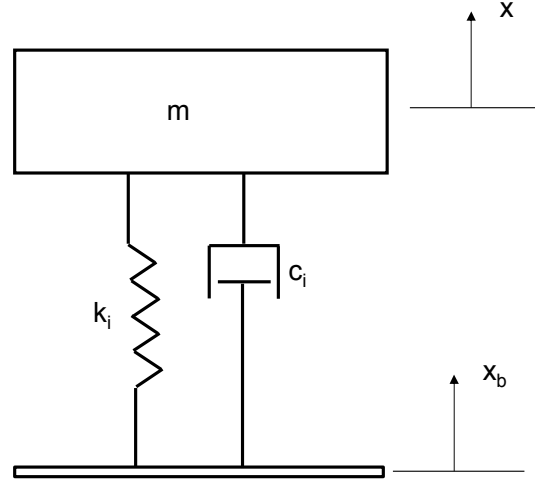
Figure 3.2: Base Excitation Model – 1 DOF.

The governing equation for the model shown in Figure 3.2 is shown in Equation 3.1.

$$m\ddot{x} + c_i\,(\dot{x} - \dot{x}_b) + k_i(x - x_b) = f \quad (3.1)$$

In Equation 3.1 and Figure 3.2, m is the mass, $k_i$ is the stiffness of the damper, and $c_i$ is the damping constant of the system. The subscript 'i' is indicative of the MR damper's ability to change its properties with the change of input current to the electromagnet. Also, $x$ is the displacement of the isolated mass (m), $x_b$ is the displacement of the base, and $f$ is the external force acting on the mass. Displacement and acceleration transmissibility are both expressed as ratios of the payload to the base, using displacement or acceleration values as appropriate. These ratios are mathematically equal, as shown in Equation 3.2 below. The second part of the equation relates the parameters from Table 3.1 and the frequency ratio (excitation frequency over natural frequency of the system) to transmissibility.

$$T_d = \frac{X}{X_b} = T_a = \frac{\ddot{X}}{\ddot{X}_b} = \left[\frac{1+(2\zeta_i r_i)^2}{\left(1-r_i^2\right)^2+(2\zeta_i r_i)^2}\right]^{\frac{1}{2}} \quad (3.2)$$

In Equation 3.2, the subscripts 'd' and 'a' refer to displacement and acceleration, respectively. $T_d$ is the displacement transmissibility and $T_a$ is the acceleration transmissibility. Also, $r_i$ is the frequency ratio between the base excitation frequency and the natural frequency. Force transmissibility ($T_f$) can be directly computed from the displacement transmissibility as:

$$T_f = r_i^2 T_d = r_i^2 T_a \qquad\qquad (3.3)$$

The capability of the damper can be assessed from displacement transmissibility and force transmissibility. However, there is an inherent trade-off between force transmissibility and displacement transmissibility for the frequency ratio of $r_i > \sqrt{2}$. This will be demonstrated further in the subsequent discussion for the damper used in this study.

### 3.4.  Modeling – Results and Discussion

The simulations for displacement and force transmissibility are presented in this section. MATLAB® has been used for all mathematical modeling. The data from Table 3.1 is used for the simulations. In the plots, the X-axis is the ratio of excitation frequency to the natural frequency of the system and the Y-axis is the transmissibility. Only four current levels are used since the stiffness ($k_i$) and damping ($c_i$) constants are not seen to change appreciably with small changes in current. The damping ratio is calculated for the two payloads that are used for experimentation, and is listed in Table 3.1. It can be seen from the data that the damping constant increases with the increasing current input while the stiffness constant does not change appreciably. This has also been reported in the existing literature. The displacement transmissibility and force transmissibility plots for the base excitation system shown in Figure 3.2, with the use of the MR damper, are shown in Figure 3.3 and Figure 3.4. As can be seen from Figure 3.3, increasing the input current reduces displacement transmissibility before the frequency ratio of $\sqrt{2}$, whereas there is an increase in displacement transmissibility with increasing input current after the frequency ratio of $\sqrt{2}$.
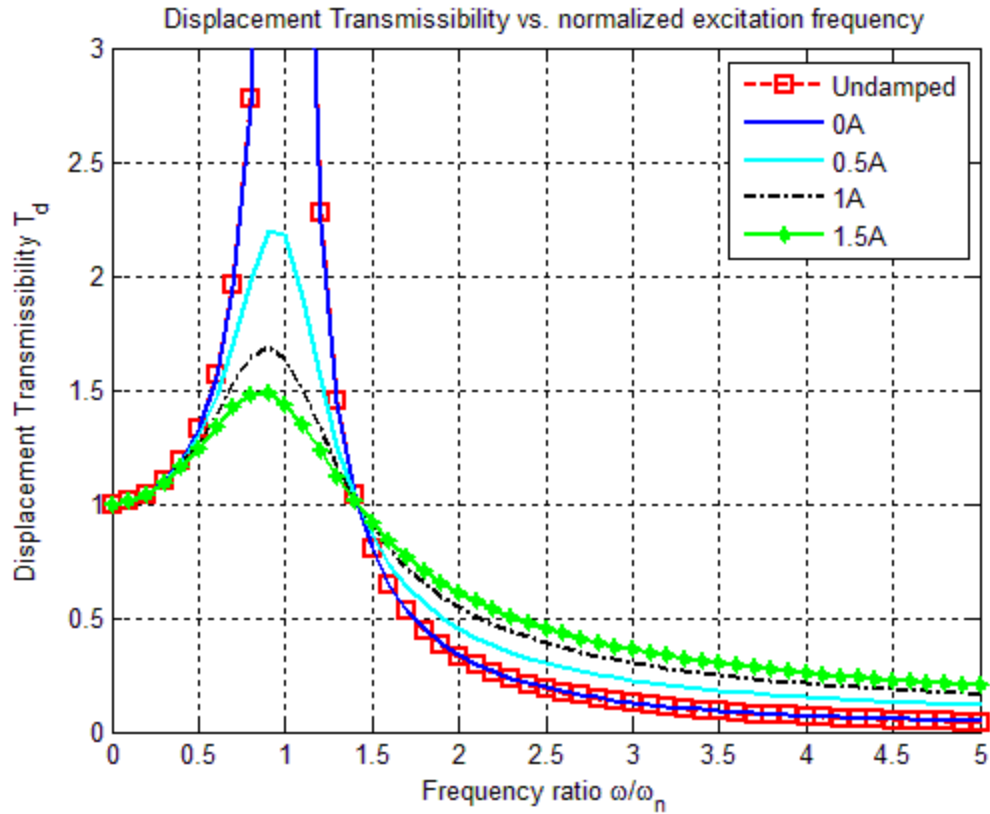
Figure 3.3: Displacement Transmissibility versus normalized excitation frequency as a function of input current.

As seen in Figure 3.3, the displacement transmissibility has a predictable shape for all the current levels, even though the magnitude of the peak varies with current applied to the damper. Beyond a frequency ratio of approximately $\sqrt{2}$, the five plots exhibit a mitigation of transmissibility, with the lower level of damping (lower current) resulting in lower transmissibility ($T_d$). It may be noted that Figure 3.3 represents acceleration transmissibility as well.
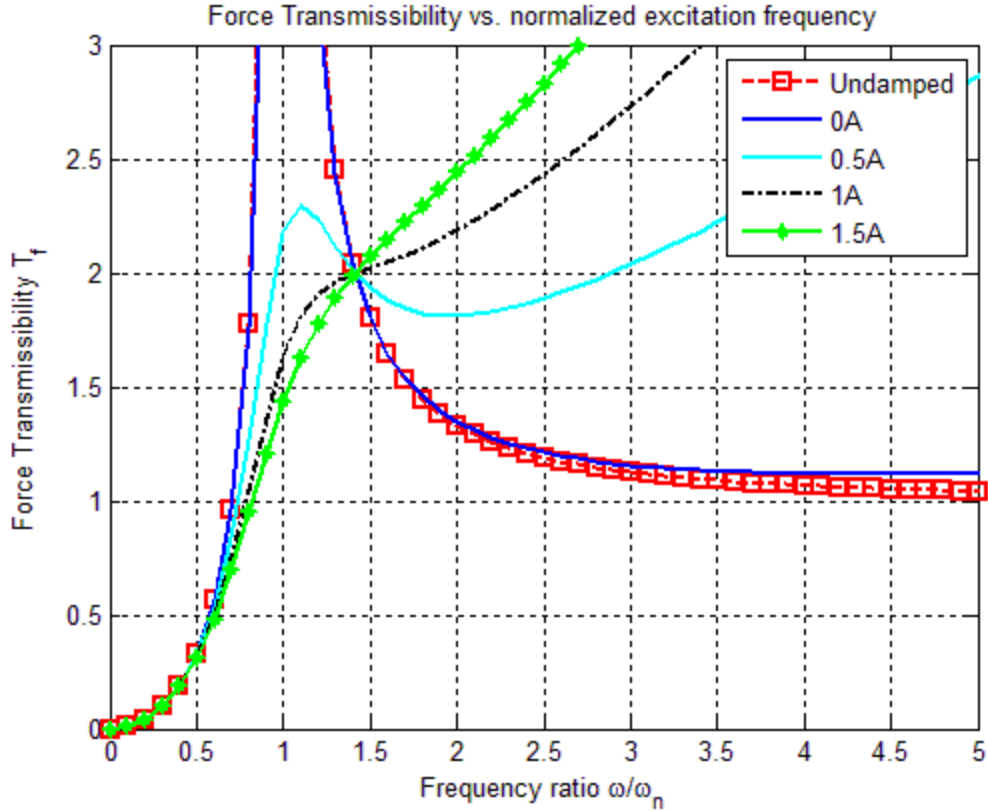
Figure 3.4: Force Transmissibility versus normalized excitation frequency as a function of input current.

Figure 3.4 shows the force transmissibility plot for the MR damper, and compares it to an undamped system. This plot shows that the change in current to the damper has a significant effect on force transmissibility over the change in frequency. With an increase in current, the force transmissibility reduces with the increase of frequency ratio until the frequency ratio of $\sqrt{2}$. The undamped system is identical to the damper with 0A current input.

### 3.5.    Conclusion

Comparing Figures 3.3 and 3.4, after reaching the frequency ratio of approximately $\sqrt{2}$, the displacement and force transmissibility characteristics of the MR damper sharply diverge from each other. While $T_d$ starts at 1, with base displacement being matched by the payload, with an increase in frequency ratio (beyond the natural frequency) $T_d$ decreases, approaching 0. Figure 3.4 shows that $T_f$ is near 0 at low frequency ratios, and increases with the natural frequency. Similar to displacement transmissibility, the

16

current level has a significant impact on the magnitude of the peak. Current level continues to have an impact on the shape of the plot beyond the natural frequency, with an increasing current level increasing the $T_f$ value. The divergence of the two models at the frequency ratio of $\sqrt{2}$ suggests a trade-off between force and displacement transmissibility beyond that frequency. The findings from the mathematical models match expectations from the relevant literature.

The behavior of the MR damper can be directly attributed to the increase in damping with the increasing input current that governs the behavior of the electromagnet of the damper. However, a crucial difference between a passive damper and the MR damper is that the damping levels can be changed continuously to meet the requirements of the isolation system with a changing payload or with a changing excitation frequency. The results from force transmissibility in Figure 3.4 are consistent with the findings from the displacement transmissibility plot, highlighting the ability of the MR damper to meet the needs of active damping. It may be noted that there are multiple models of an MR damper in the existing literature, particularly in order to represent hysteresis and saturation behavior over large displacement amplitudes. However, the focus of this study is on small amplitudes of displacements. Therefore, these models have not been used for the purposes of this study.

CHAPTER 4 :   EXPERIMENTAL RESULTS


This chapter presents the highlights of the experimental results obtained during the course of the study. The steps involved in planning and executing the experimental work are also included. The results are analyzed and discussed in detail.

## 4.1.    Damper Characterization

The magnetorheological (MR) damper used in this study was procured from LORD Corporation. This is a mono-tube damper (RD-8041-1) with a maximum stroke length of 74 mm, a body diameter of 42.1 mm and a maximum extended length of 248 mm. The input current to the electromagnet can be varied up to a maximum of 2 A with an intermittent input, and up to 1.5 A with a constant input. The MR damper and the controller kit used in this study are shown in Figure 4.1.



Figure 4.1: MR Damper and Control Kit.


The damper used in this study was characterized in order to establish a baseline that could be used to comprehend the behavior of the damper. The characterization results were used to identify the stiffness behavior of the damper at different input currents to the electromagnet. Since the MR damper

exhibits a semi-active behavior, it is essential to characterize the damper at different levels of input

current. A series of tests were performed on a Universal Tensile Testing machine (also called as the

tensile tester). The tensile tester used for these tests is manufactured by Instron (Model No: 5967). A

picture of the test setup used for damper characterization is shown in Figure 4.2.  It may be noted that

mounting pins had to be manufactured to clamp the upper and lower end of the damper to the two

grippers of the tensile testing machine, as shown in Figure 4.2.



Figure 4.2: Test setup for damper characterization.

The use of the mounting pins prevented possible damage to the eyes of the damper, and allowed for some

freedom of rotation. The damper was placed as vertically as possible within the grippers. The following

loading procedure was followed for the testing:

- Turn on machine and computer, turn on compressed air line for the grippers;

- Insert a pin into upper (rod end) eye of the damper and place upper end of damper with the pin in

  the gripper, ensuring that the faces of the pin contact the surfaces of the grippers, allowing

  rotation of the damper body;

- Close the upper gripper and open the lower gripper;

19

- Lower the upper cross member, allowing the lower damper eye with the inserted pin to descend;

- Stop movement when lower pin/eye is at an appropriate height to have its faces entirely contacted by the gripper surface;

- Close the lower gripper, ensuring that only the faces of the pin are contacted;

- Move the grippers by 10 mm (closer to each other) to ensure that the damper will not be damaged by accidental over-extension during testing.

This test procedure ensured that testing is performed midway through the damper stroke. The damper was firmly held by the grippers of the tensile tester, and the test was conducted in compression. The variables of interest during this test were the compression rate and the compression force along with the current supplied to the damper through the controller kit. Relative to full extension, the test range was from 10 mm to 40 mm of compression. It may be noted that the damper has a maximum stroke length of 54 mm. The testing can be classified into two categories: constant velocity and constant force.

The tests with a constant velocity setting had a response variable of force exerted by the damper. The load was applied at a variable rate ranging from 10 to 20 mm/min. The input current for the electromagnet of the damper was varied from 0 to 1.5 A in various increments. The increments and the variables associated with this test are listed in Table 4.1.

Another series of tests was conducted in order to focus on applying a constant force so as to determine an appropriate payload for the damper when it is used for testing on the shaker table. This is specifically important because the damper has an in-built gas charged accumulator. Tests were performed at multiple constant loads and the current to the electromagnet of the damper was varied.

Table 4.1: Damper Characterization – list of test runs.

| Amperage (A) | Rate (N) | Amperage (A) | Rate (N) | Amperage (A) | Rate (mm/min) |
|---|---|---|---|---|---|
| 0.0 | 10 | 0.25 | 10 | 0.1 | 10 |
| 0.5 | 10 | 0.125 | 10 | 0.125 | 10 |
| 1 | 10 | 0.375 | 10 | | |
| 1.5 | 10 | | | | |
| Amperage (A) | Rate (mm/min) | Amperage (A) | Rate (N) | Amperage (A) | Rate (mm/min) |
| 0 | 10 | 0 | 15 | 0 | 20 |
| 0.1 | 10 | 0.1 | 15 | 0.1 | 20 |
| 0.2 | 10 | 0.2 | 15 | 0.2 | 20 |
| 0.3 | 10 | 0.3 | 15 | 0.3 | 20 |
| 0.4 | 10 | 0.4 | 15 | 0.4 | 20 |
| 0.5 | 10 | 0.5 | 15 | 0.5 | 20 |
| 0.6 | 10 | 0.6 | 15 | 0.6 | 20 |
| 0.7 | 10 | 0.7 | 15 | 0.7 | 20 |
| 0.8 | 10 | 0.8 | 15 | 0.8 | 20 |
| 0.9 | 10 | 0.9 | 15 | 0.9 | 20 |
| 1 | 10 | 1 | 15 | 1 | 20 |

Some of the test results obtained from the damper characterization are shown in Figure 4.3 and Figure 4.4. It can be discerned from the force-displacement characteristics that the damper stiffness increases as the input current to the electromagnet increases. Also, the saturation level is seen to increase with the increasing strain rate. Note that in both Figures, the "0A' and "0.1A" lines overlap significantly.
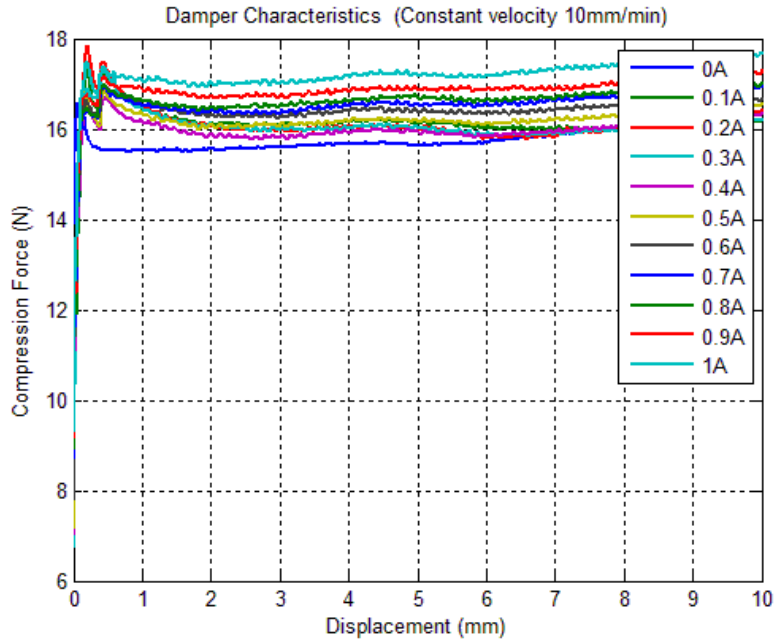
Figure 4.3: Force-displacement characteristics (at 10 mm/min).
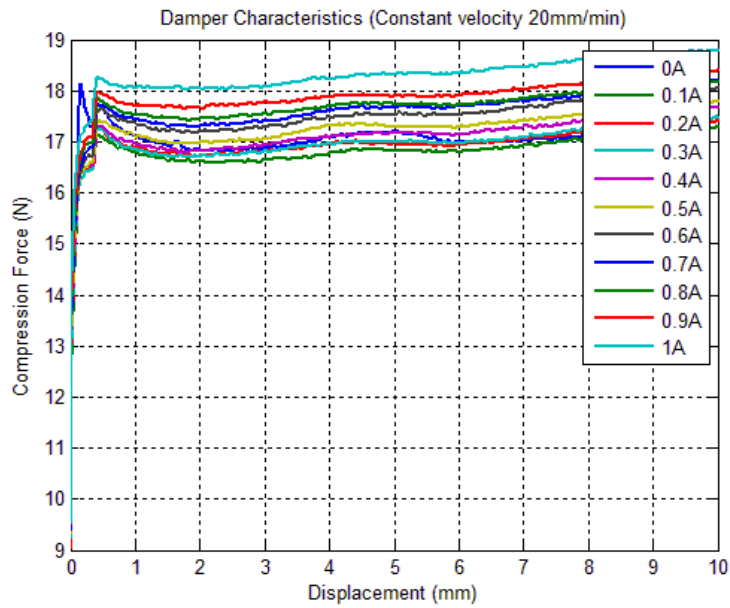


Figure 4.4: Force-displacement characteristics (at 20 mm/min).

The damper parameters identified from the characterization test discussed above are shown in Table 4.2.

Only four current levels are used since the stiffness ($k_i$) and damping ($c_i$) constants are not seen to change

appreciably with small changes in current. The damping ratio is calculated for the two payloads that were used for experimentation in shaker testing. It can be seen from the data that the damping constant increases with the increasing current input while the stiffness constant does not change appreciably. This has also been reported in the existing literature [7].

Table 4.2: Damper Parameters – two configurations.

| Current (A) | $k_i$ (N/m) | $c_i$ (N-s/m) | $\zeta_i$ ($m = 11.5$ kg) | $\zeta_i$ ($m = 14.9$ kg) |
|---|---|---|---|---|
| 0 | 100 | 2.5 | 0.037 | 0.032 |
| 0.5 | 150 | 20 | 0.240 | 0.211 |
| 1 | 150 | 30 | 0.361 | 0.317 |
| 1.5 | 150 | 37.5 | 0.451 | 0.396 |

The damper characterization discussed in this section is used to develop the shaker table test that will be discussed in Section 4.2.

## 4.2.    Shaker Table Testing

A layout of the experimental setup used for the shaker table testing is shown in Figure 4.5. The shaker table that was used to generate the excitation for this experiment is an Unholtz Dickie model S452 LP (low profile), with a model SA-15 control unit.
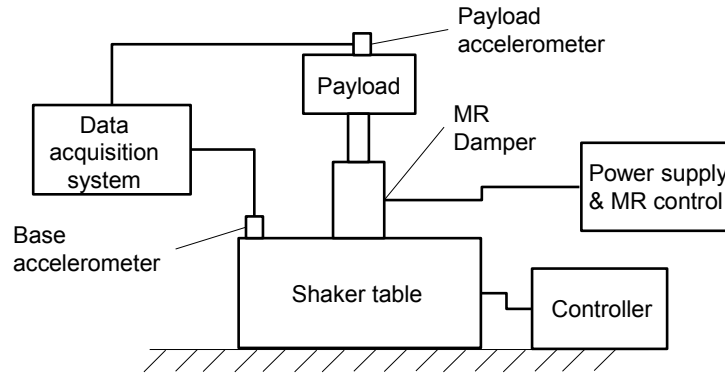


Figure 4.5: Experimental setup – block diagram.

As shown in Figure 4.5, The MR damper is connected to the single degree-of-freedom shaker table to provide base excitation. The piston end of the damper is assembled to the payload and the other

end of the damper is securely assembled to the top plate of the shaker table. Accelerometers are connected to the top plate of the shaker table as well as the payload. Both accelerometers are connected to the data acquisition system. The electromagnet of the MR damper is connected to the controller kit that is in turn connected to a DC power supply. A National Instruments c-DAQ-9172 with a NI 9234 accelerometer module is used for data collection at a sampling frequency of 1600 Hz. A pair of Dytran 3019A accelerometers are used in conjunction with their respective power amplifiers. The shaker table is driven by its controller through a function generator. An Agilent 33220A 20 MHz Function/Arbitrary waveform generator was connected to the control unit, and was used to generate the input signal for the shaker table testing. The armature, the driven part of the shaker, has a pattern of mounting studs permanently attached to the surface, with each stud having a 3/8-16 threaded hole. It may be noted that data collection is started after several cycles of excitation in order to allow the system to settle. A picture of the entire test setup is shown in Figure 4.6.
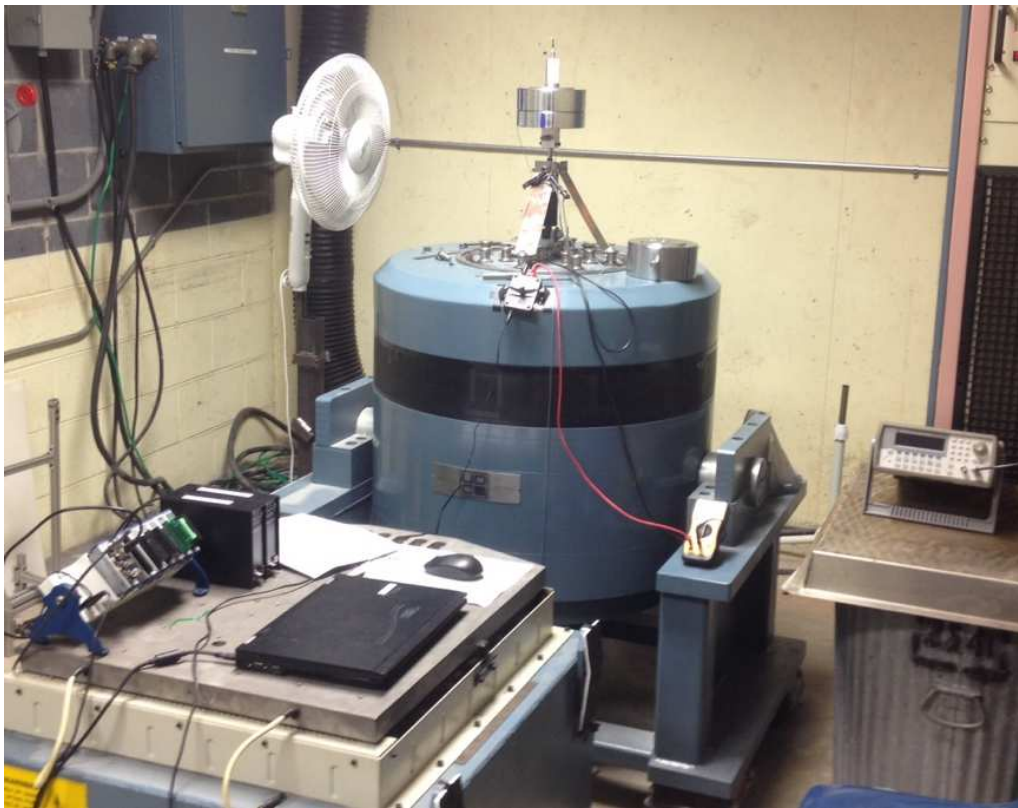


Figure 4.6: Shaker table test setup.

Several components were fabricated in order to assemble the test setup. To connect the lower eye of the damper to the table, a bracket was designed and milled. A mounting bolt was inserted through a hole in the bracket to connect the damper to the top surface of the shaker table. In order to keep the damper upright, an aluminum collar was fabricated. This collar was pocketed by using a milling machine in order to make an interior diameter equal to the outside diameter of the damper body. A slot was cut through the collar, and a screw was threaded into it so that the tension on the damper could be adjusted. Initially, a single support bracket was made out of aluminum to limit movement in the axis not constrained by the damper eye. While this setup did limit unwanted motion of the damper, there was an excessive side-to-side movement, especially with a payload and with input vibration from the shaker table. Such a degree-of-freedom could have potentially introduced errors into accelerometer data collection, or even damaged the damper. A new set of braces was fabricated to support the damper. A picture of the fixture fabricated to support the damper is shown in Figure 4.7.
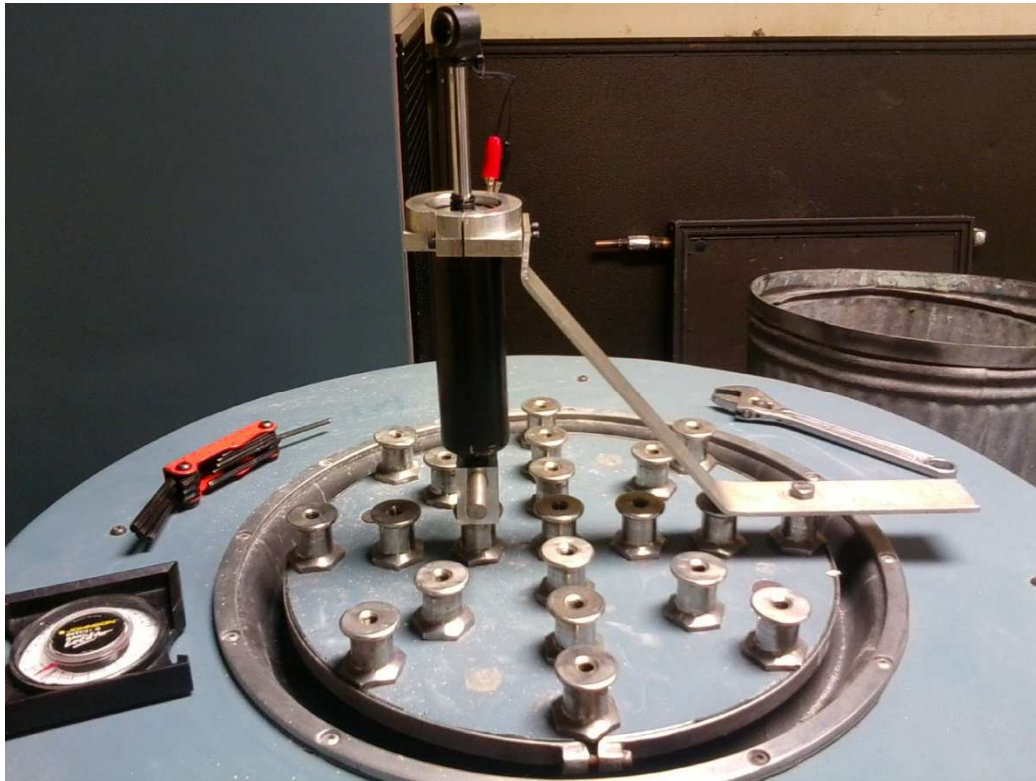


Figure 4.7: Damper support fixture – partial assembly.

To enhance the rigidity of the damper support, an additional support was provided. With these supports, the damper could be centered on the table, with the braces oriented at 90 degrees from each other. This design located the damper rigidly without providing an additional degree-of-freedom even after assembling the payload and providing vibrational inputs from the shaker. The final supporting fixture is shown in Figure 4.8.



Figure 4.8: Damper support fixture – complete assembly.

The payloads for testing were made from a combination of weights, these were selected based on availability and the overall payload capability of the shaker. The payload weights were built from a combination of 10 kg, 6.6 kg and 4.9 kg weights. These weights were used to provide payloads of 11.5 Kg and 14.9 Kg for testing. To secure the range of weights to the top of the damper, an aluminum bracket was made. This bracket fit over the upper eye of the damper, and had a pin pass through the eye and the bracket to hold them together. Set screws were tapped into the lower part of the bracket to prevent any relative rotation between the bracket and the damper. A bolt was inserted through the top of the bracket,

and passed through a plate and the payload weights. The accelerometer fixture for the payload was a threaded block that went onto the end of the rod, securing the payload. The complete payload assembly with the accelerometer is shown in Figure 4.9.
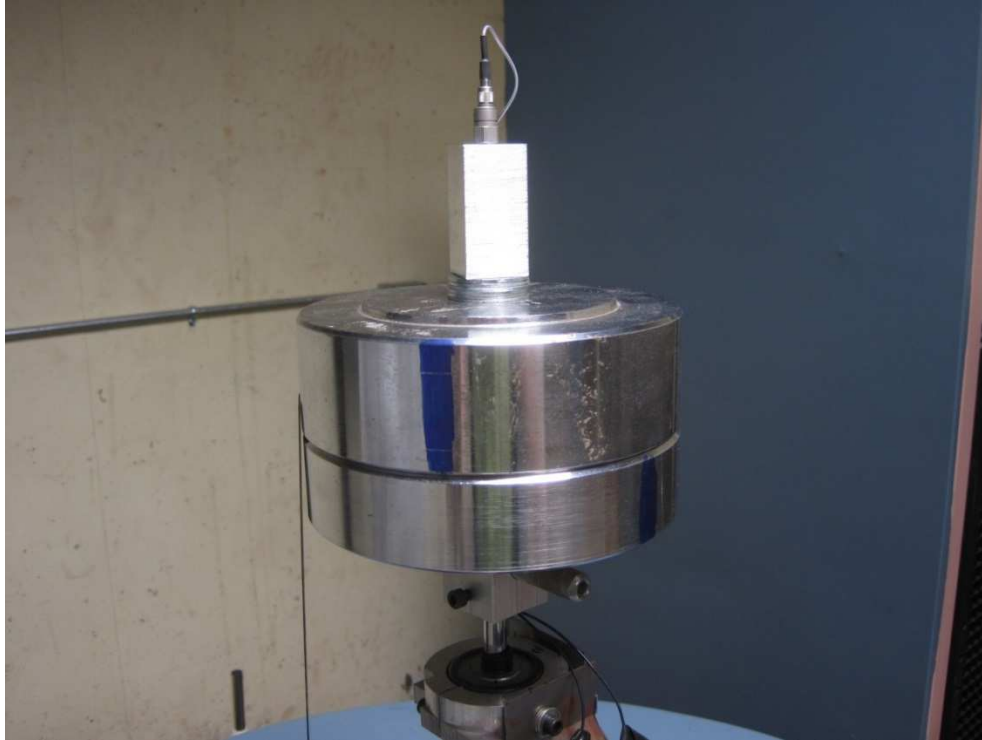


Figure 4.9: Payload assembly.

The two accelerometers used to measure acceleration during this study were mounted so as to allow a comparison of the input excitation with the acceleration experienced by the payload. The accelerometer mounted on the shaker table was threaded into an insert that had internal ¼-28 threads to match the accelerometer, and 3/8-16 external threads to match the integrated studs on the shaker table. As mentioned earlier, and shown in Figure 4.9, the payload accelerometer was threaded directly into a block that also acted as a nut to secure the payload to the payload bracket and the upper damper eye. Both accelerometers were connected to power amplifiers, and then to the data acquisition system through coaxial cables.

A National Instruments c-DAQ-9172 unit with a NI 9234 accelerometer module was used to collect the acceleration data through LabView. Each data set was output into a folder with the log name as the label, and each folder contained three files: a TDMS file, which was the log file and could be opened using Microsoft Excel; a TDMS_INDEX file used by the software, and a text file that contained the metadata about the data set, the log name and description, number of samples, log duration, and other information. Figure 4.10 shows a screen shot of the software interface. Each data collection run was conducted so as to record analog acceleration signals from two channels '0' and '1' (from the base and the payload respectively). The settings for both channels were identical. The voltage output from the accelerometers was discretized at the sampling frequency in terms of millivolts (mV) with a sensitivity of 10 mV/g, as seen in Figure 4.10. It may be noted that the unit 'g' represents acceleration due to gravity (9.81 m/s$^2$), and is a commonly used unit in acceleration measurements. A screen shot of the live data collection is shown in Figure 4.11.
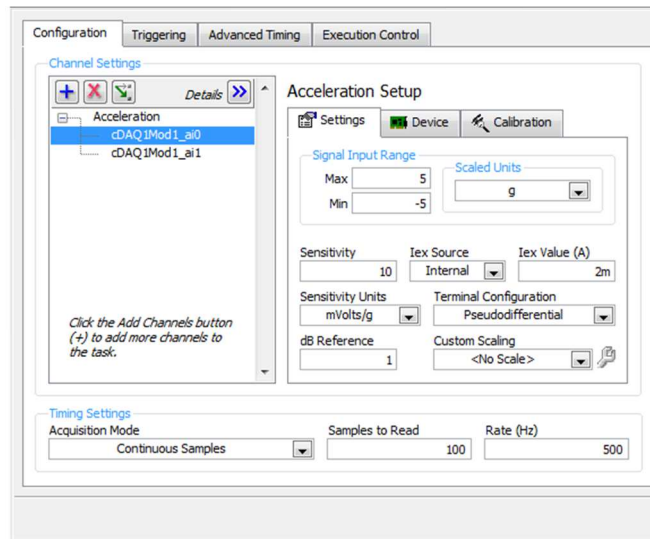


Figure 4.10: Screen shot of shaker table data collection settings.
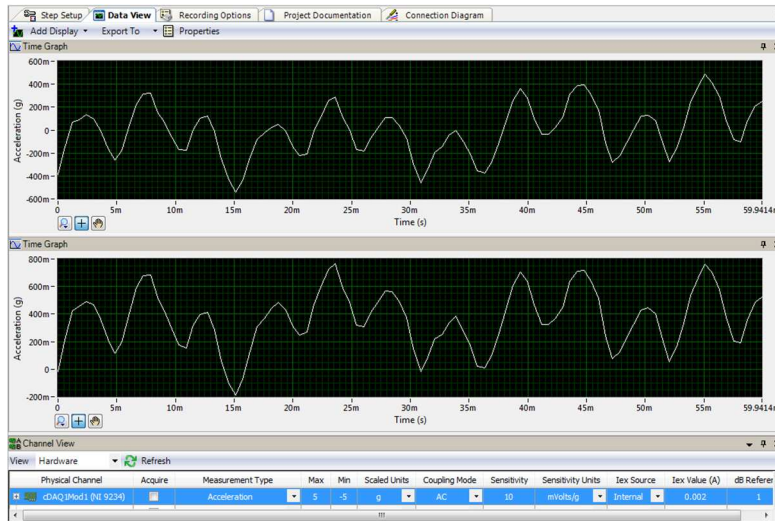
Figure 4.11: Screen shot of shaker table acceleration data collection.

In Figure 4.11, the top graph displays data from channel 0 (base acceleration), and the lower graph displays data from channel 1 (payload acceleration).

For all the test runs, the shaker table input was provided by the frequency generator through the controller. The damper was controlled separately by the control module, and the input current to the electromagnet of the damper was measured by a multimeter. The overall test setup corresponds to the block diagram shown in Figure 4.5. All post-processing of the data was performed in MATLAB. The post-processing consisted of filtering the data, transforming the time domain data into frequency domain, and calculating metrics such as the root mean square (RMS) and the peak values of acceleration to evaluate vibration mitigation capability of the damper. The output of all the test runs is shown in the next section. The testing on the shaker table consisted of two main settings – constant frequency, and frequency sweep. Table 4.3 shows a list of the settings used for each variable.

Table 4.3: Test Settings (shaker table).

| Amplitude (mVpp) | 100 | | 200 | | 300 | | 400 | | 600 | |
|---|---|---|---|---|---|---|---|---|---|---|
| Static Frequency (Hz) | 5 | | 10 | | 15 | | 20 | | 25 | 30 |
| Frequency Sweeps (Hz) | 2-40 | | | | 5-50 | | | 9-16 | | |
| Current (amps) | 0.0 | 0.2 | 0.4 | 0.5 | 0.6 | 0.7 | 0.8 | 1.0 | 1.2 | 1.5 |
| Payload (Kg) | 11.5 | | | | | 14.9 | | | | |

All tests runs lasted for two to three minutes. Due to the possibility of an increase in the fluid temperature during testing, a fan was used during the test runs and temperature was monitored during testing. The temperature was found to be remain within 65 to 75 degrees Fahrenheit. After the first few runs, the temperature was not recorded any more since the temperature did not vary significantly.

As seen in Table 4.3, two types of runs were made using the shaker table – constant frequency runs, and runs with frequency sweeps.

### 4.3.    Damping Results

This section summarizes all the results. Although a large number of runs were performed at varying amplitudes and frequencies, a limited amount of data is presented in this section to showcase the main findings about the capability of the damper.

Figures 4.12 through 4.14 show typical results from the constant frequency testing. The results indicate that acceleration levels were generally reduced between the table and payload, as seen in the time response as well as the frequency response. There is no shift in frequency, as seen from the frequency response, but the accelerations are mitigated. Figure 4.12 shows a comparison between the acceleration of the table (or base) and the acceleration of the payload in the time domain when the base is excited at 10 Hz. As can be clearly discerned, the acceleration of the payload is significantly mitigated.
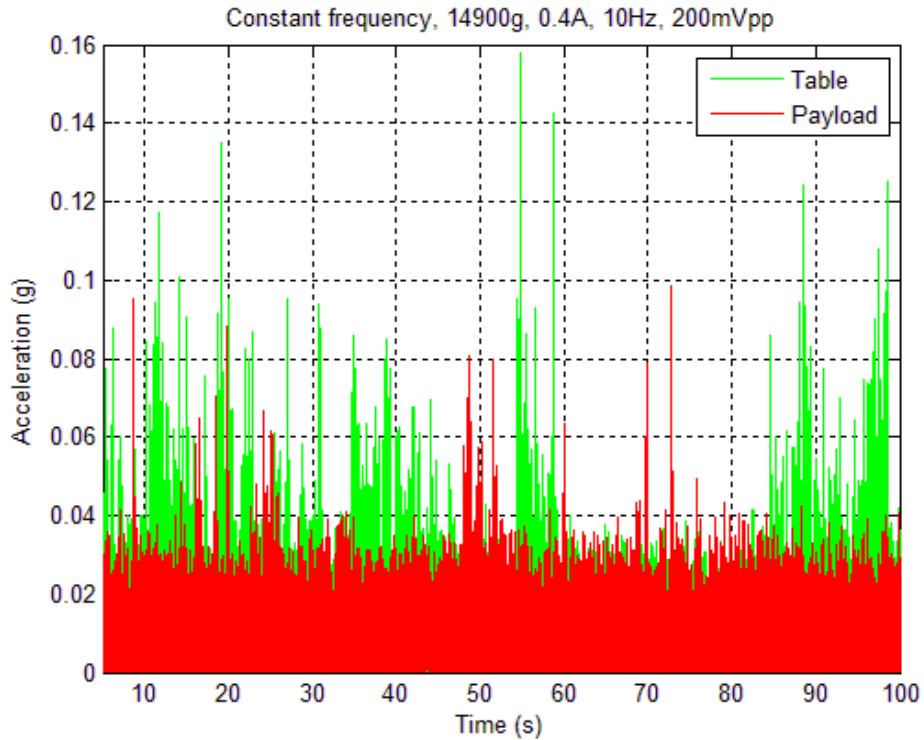
Figure 4.12: Acceleration versus time for a constant excitation frequency (10 Hz, 200mVpp), input current of 0.4A, payload of 14.9 kg.

Figure 4.13 shows the comparison of the data shown in Figure 4.12 in the frequency domain. The ability of the damper to mitigate vibration is again apparent, as seen by the significantly lower amplitude of the payload response in the frequency domain. Figure 4.14 shows a hysteresis plot to further compare the base acceleration amplitude with the payload acceleration. The difference between the ranges of acceleration amplitudes can be examined from the hysteresis plot.
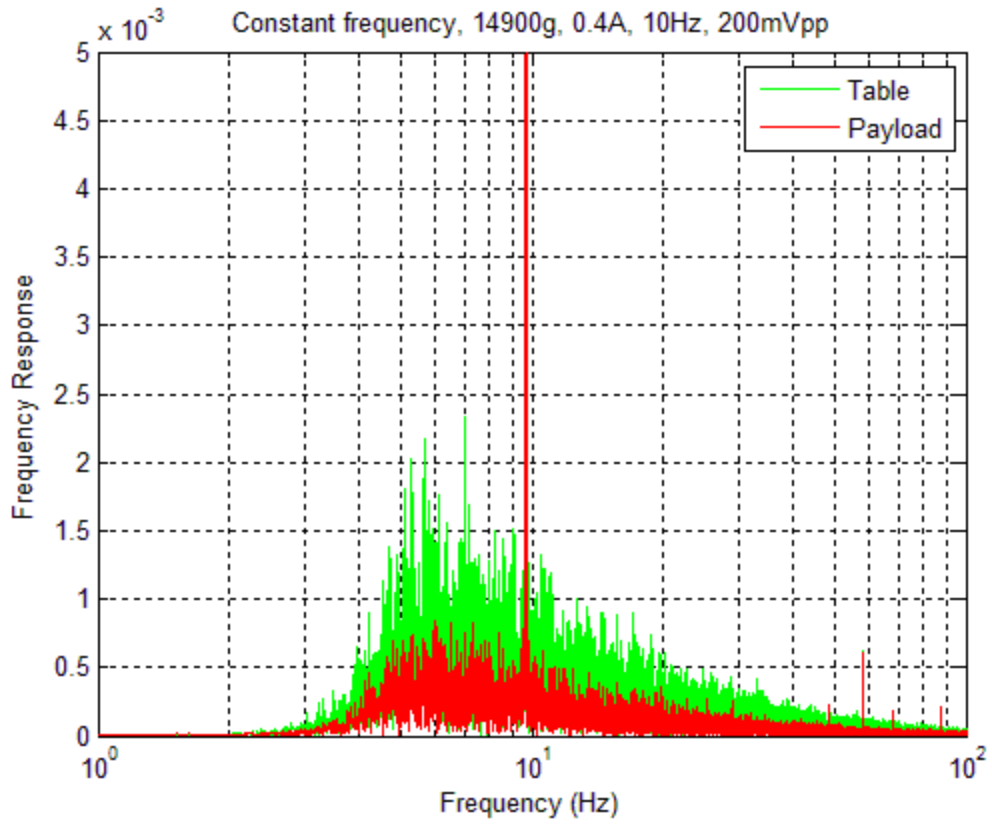
Figure 4.13: Frequency response plot (logarithmic scale) for constant excitation frequency (10 Hz, 200mVpp), input current of 0.4A, payload of 14.9 kg.
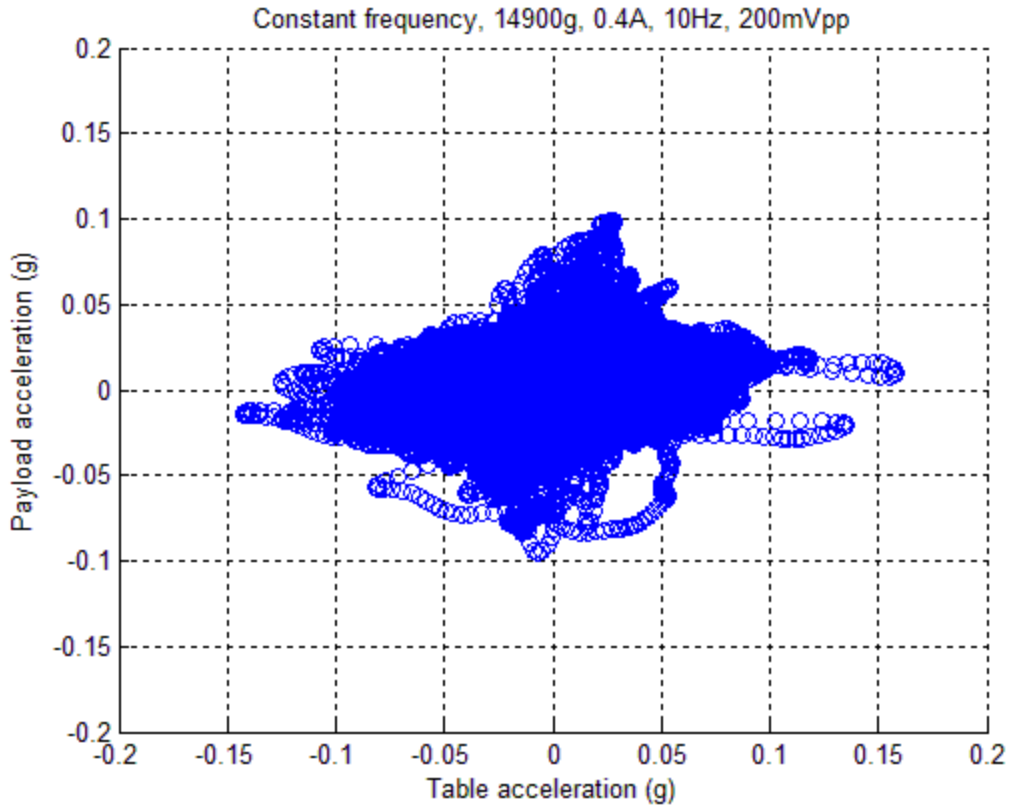
Figure 4.14: Hysteresis plot for constant excitation frequency (10 Hz, 200mVpp), input current of 0.4A, payload of 14.9 kg.

It may be noted that the frequency response in Figure 4.13 regards to the magnitude of acceleration in the frequency domain.  Output from some more test runs is shown in the subsequent part of this section, particularly from the test runs involving a frequency sweep from 9 to 16 Hz. Figures 4.15 and 4.16 show one such result for a payload of 11.5 kg in the time and frequency domains respectively. Some vibration mitigation can be seen from the time domain results in Figure 4.15, and multiple peaks are observed in Figure 4.16 since the input excitation covers a range of frequency. Mitigation is seen to be higher in certain frequency ranges due to the inherent natural frequency of the system being tested. This will be discussed further.
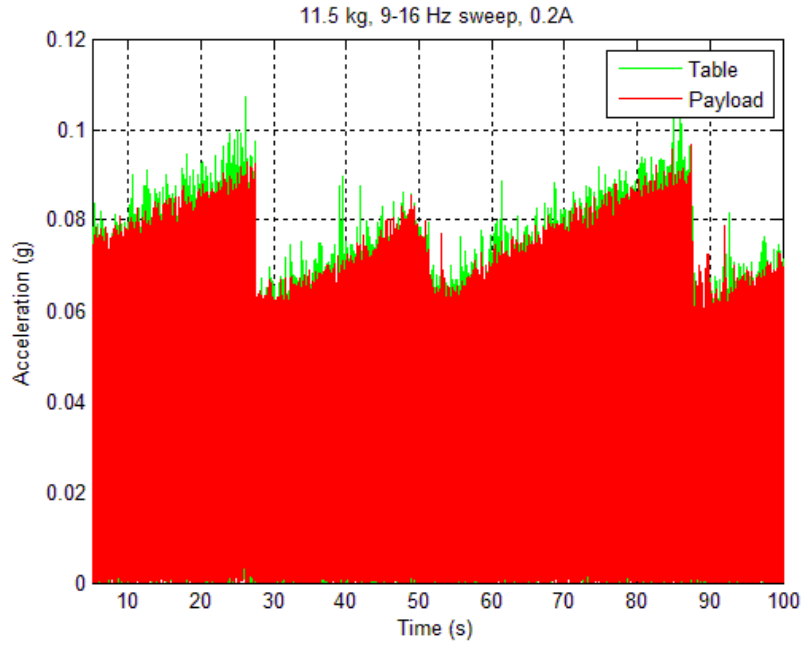
Figure 4.15: Acceleration versus time for a payload of 11.5 kg, damper current of 0.2A, frequency sweep from 9-16 Hz, amplitude of 400 mVpp.



Figure 4.16: Frequency response plot, logarithmic scale; payload of 11.5 kg, damper current of 0.2A, frequency sweep from 9-16 Hz, amplitude of 400 mVpp.

Figure 4.17 shows a hysteresis plot to compare the ranges of acceleration between the payload and the base. This plot does not show an appreciable difference between the ranges of acceleration. However, these results can be interpreted better by comparing peak accelerations and RMS accelerations at several input currents. This will be discussed in the subsequent part of this section.
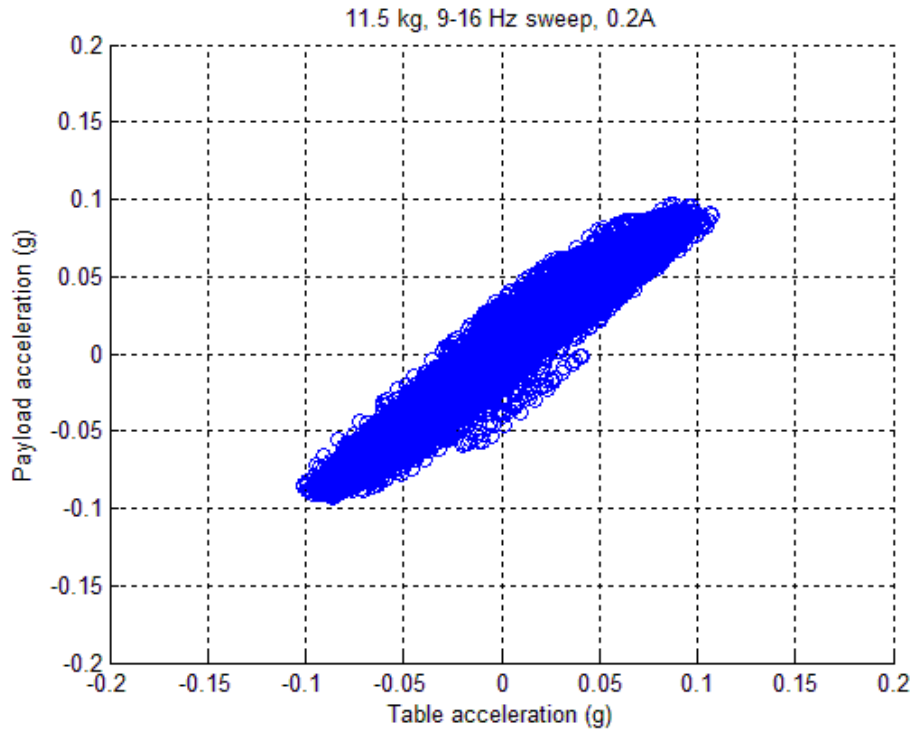


Figure 4.17: Payload acceleration versus table acceleration plot; payload of 11.5 kg, damper current of 0.2A, frequency sweep from 9-16 Hz, amplitude of 400 mVpp.

Another set of test results is shown in Figures 4.18 through 4.20. The main distinction between these results and the results in Figures 4.15 through 4.17 is that the input current to the electromagnet of the damper has been increased from 0.2 A to 0.7 Hz. Although there is no appreciable difference between the two set of results in the time and frequency domains, a comparison of the maximum and RMS levels of acceleration will demonstrate that the increase in the current enhances damping.
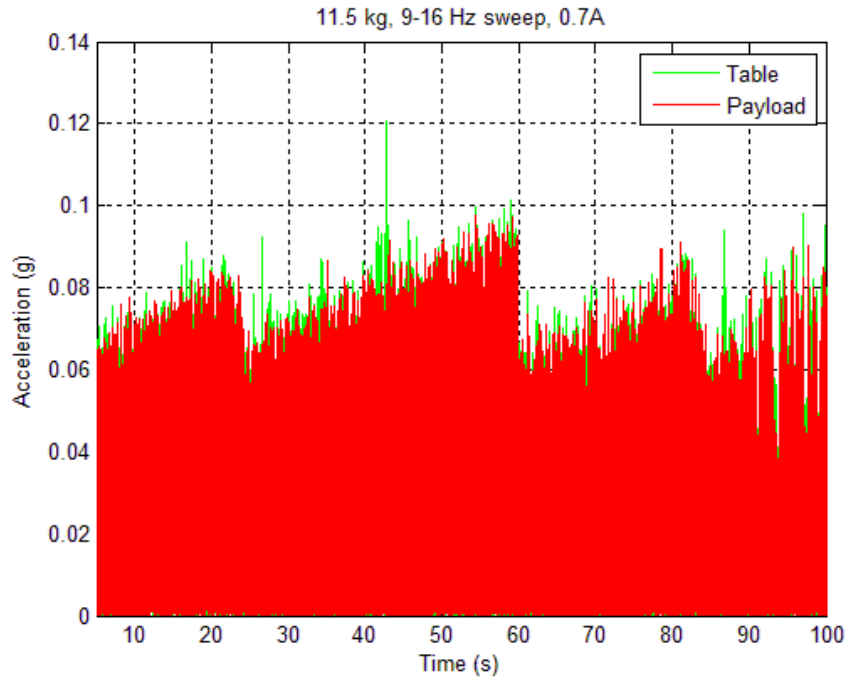
Figure 4.18: Acceleration versus time plot; payload of 11.5 kg, damper current of 0.7A, frequency sweep from 9-16 Hz, amplitude of 400 mVpp.
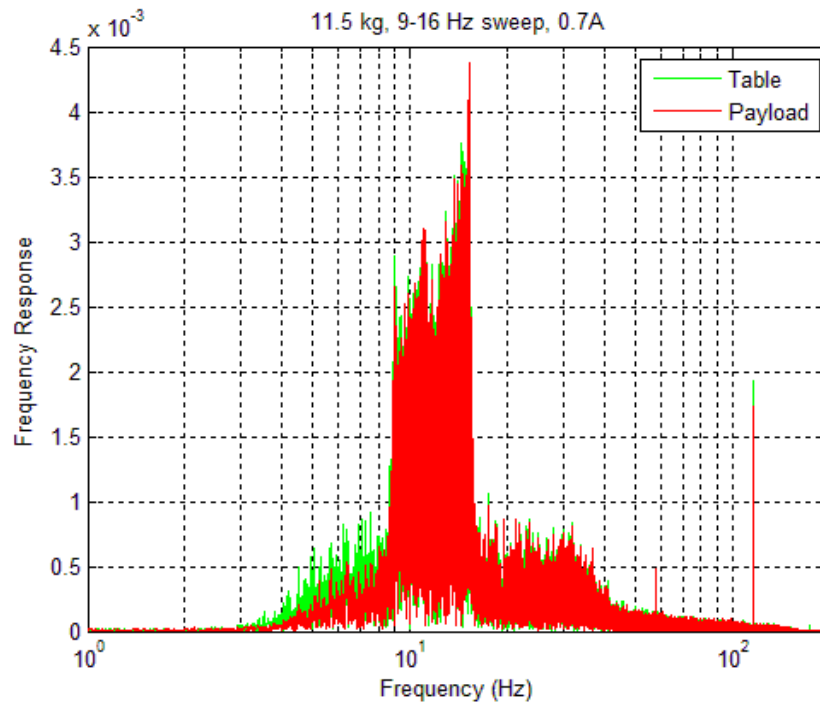


Figure 4.19: Frequency response plot, logarithmic scale; payload of 11.5 kg, damper current of 0.7A, frequency sweep from 9-16 Hz, amplitude of 400 mVpp.
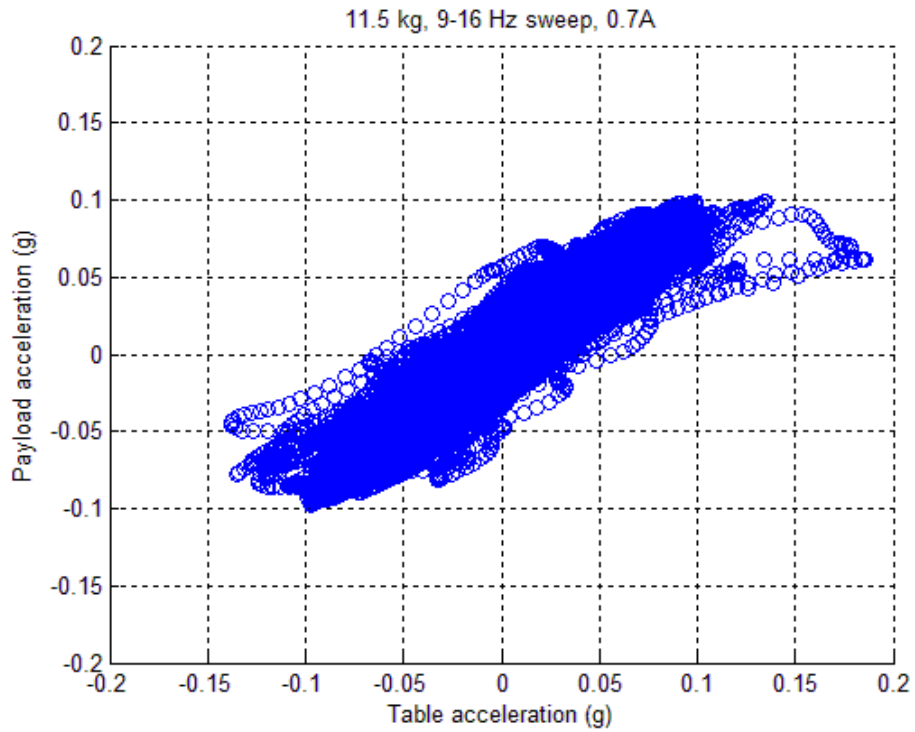
Figure 4.20: Payload acceleration versus table acceleration plot; payload of 11.5 kg, damper current of 0.7A, frequency sweep from 9-16 Hz, amplitude of 400 mVpp.

Two more sets of results are shown in Figures 4.21 through 4.23 and Figures 4.24 through 4.26 for the higher payload at two distinct current levels. Similar conclusions can be drawn from these additional sets.
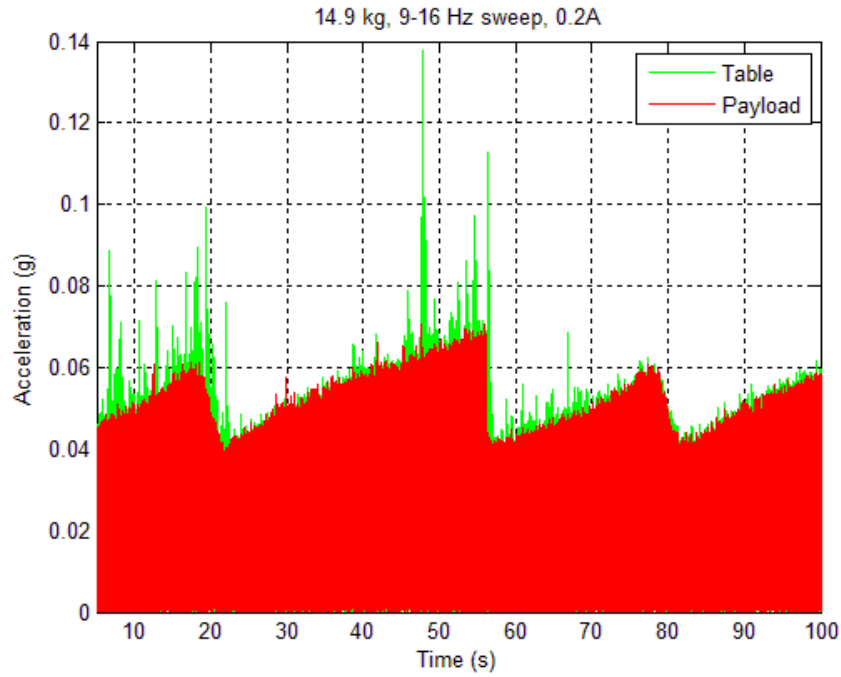
Figure 4.21: Acceleration versus time plot; payload of 14.9 kg, damper current of 0.2A, frequency sweep from 9-16 Hz, amplitude of 400 mVpp.
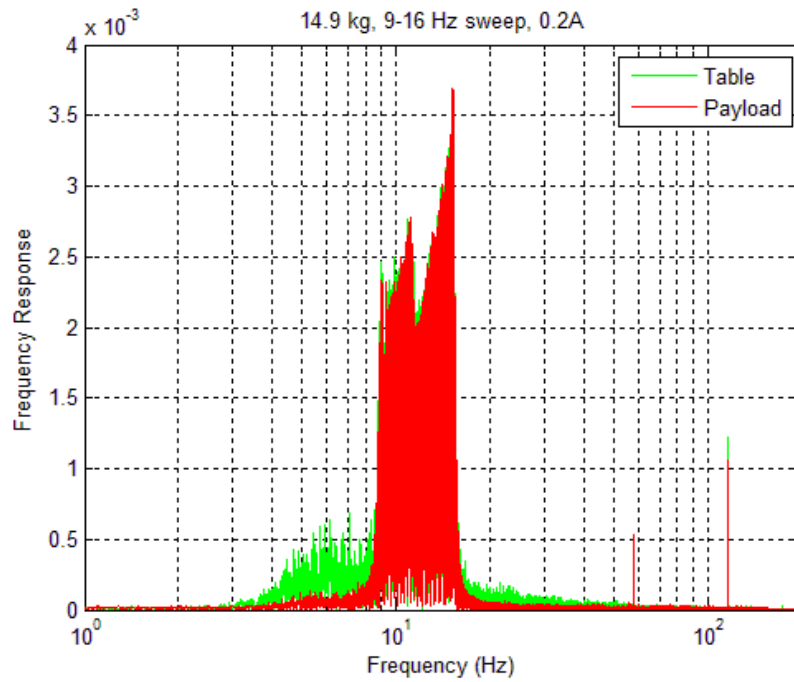


Figure 4.22: Frequency response plot, logarithmic scale; payload of 14.9 kg, damper current of 0.2A, frequency sweep from 9-16 Hz, amplitude of 400 mVpp.
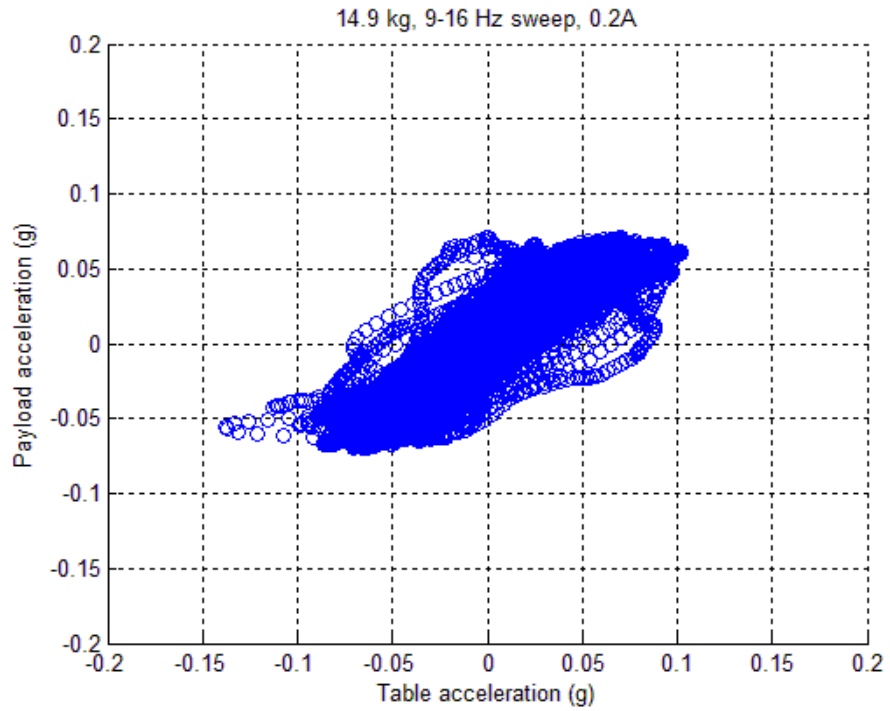
Figure 4.23: Payload acceleration versus table acceleration plot; payload of 14.9 kg, damper current of 0.2A, frequency sweep from 9-16 Hz, amplitude of 400 mVpp.
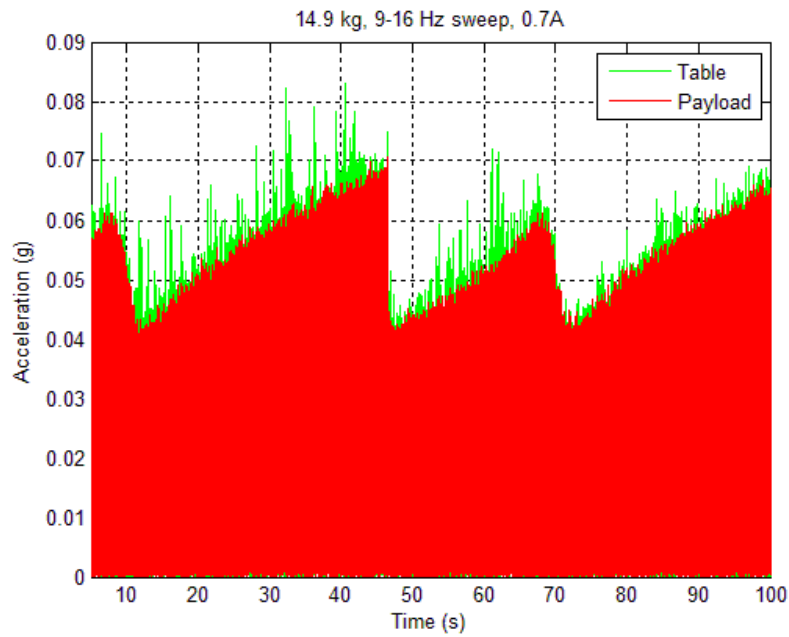


Figure 4.24: Acceleration versus time plot; payload of 14.9 kg, damper current of 0.7A, frequency sweep from 9-16 Hz, amplitude of 400 mVpp.
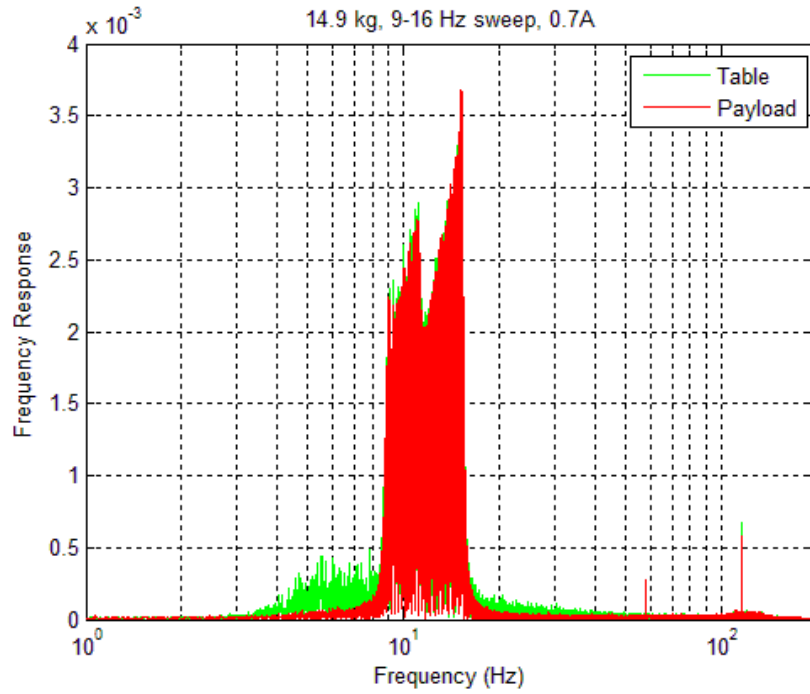
Figure 4.25: Frequency response plot, logarithmic scale; payload of 14.9 kg, damper current of 0.7A, frequency sweep from 9-16 Hz, amplitude of 400 mVpp.
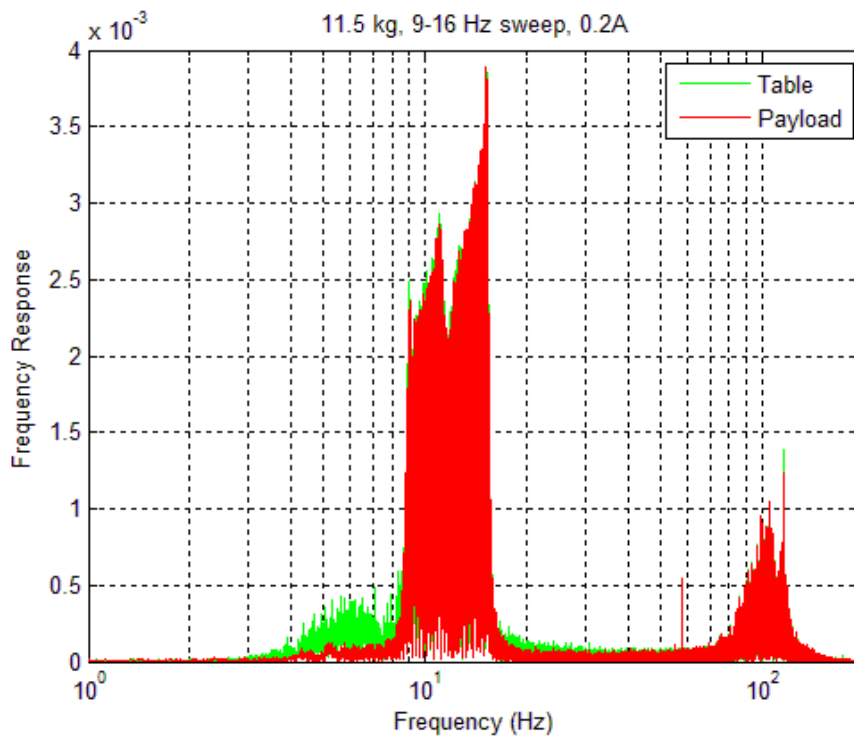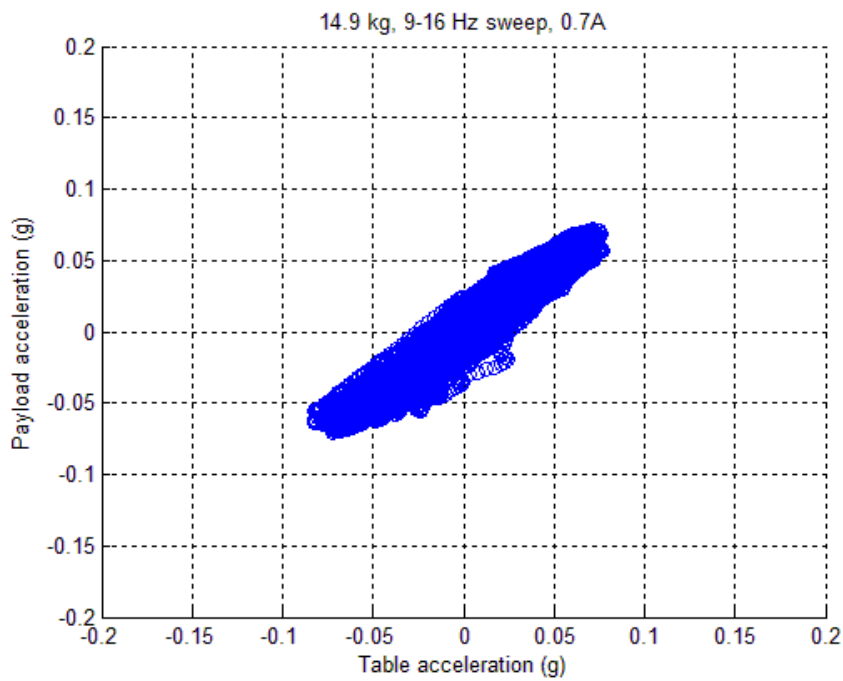


Figure 4.26: Payload acceleration versus table acceleration plot; payload of 14.9 kg, damper current of 0.7A, frequency sweep from 9-16 Hz, amplitude of 400 mVpp.

The RMS and peak values of acceleration are computed to compare the levels of acceleration

between the base and the payload. This is done to objectively analyze the test results obtained from

different levels of input current, and in order to comprehend the capability of the damper. Table 4.4

summarizes this comparison for all the runs that were performed for an input of frequency sweeps

between 9 and 16 Hz. All the accelerations in the Table 4.4 are in units of g. It may be noted that the data

presented in this table are not exhaustive, and do not present all the data that were collected as part of this

study. This table is being used to represent some of the highlights of the results obtained during the

testing performed on the shaker table.

Table 4.4: Comparison – RMS and maximum acceleration.

| Root Mean Square (RMS) Acceleration Values, in units of 'g' | | | | | | | | | |
| Payload of 11.5 kg | | | | | Payload of 14.9 kg | | | | |
| | | Amplitude (mVpp) | | | | | Amplitude (mVpp) | | |
| Current (A) | Location | 200 | 400 | 600 | Current (A) | Location | 200 | 400 | 600 |
|---|---|---|---|---|---|---|---|---|---|
| 0 | Base | | 0.0398 | | 0 | Base | | | |
| 0 | Payload | | 0.0403 | | 0 | Payload | | | |
| 0.2 | Base | | 0.0411 | | 0.2 | Base | | 0.0367 | |
| 0.2 | Payload | | 0.0408 | | 0.2 | Payload | | 0.0364 | |
| 0.4 | Base | | 0.0414 | | 0.4 | Base | | 0.0364 | |
| 0.4 | Payload | | 0.0408 | | 0.4 | Payload | | 0.0364 | |
| 0.5 | Base | 0.0190 | 0.0421 | 0.0553 | 0.5 | Base | 0.0186 | 0.0371 | |
| 0.5 | Payload | 0.0184 | 0.0410 | 0.0550 | 0.5 | Payload | 0.0193 | 0.0366 | |
| 0.6 | Base | | 0.0414 | | 0.6 | Base | | 0.0367 | |
| 0.6 | Payload | | 0.0409 | | 0.6 | Payload | | 0.0365 | |
| 0.7 | Base | 0.0189 | 0.0414 | 0.0550 | 0.7 | Base | | 0.0367 | |
| 0.7 | Payload | 0.0183 | 0.0408 | 0.0550 | 0.7 | Payload | | 0.0365 | |
| 1 | Base | | | | 1 | Base | | 0.0477 | |
| 1 | Payload | | | | 1 | Payload | | 0.0367 | |
| 1.5 | Base | | | | 1.5 | Base | | 0.0372 | |
| 1.5 | Payload | | | | 1.5 | Payload | | 0.0369 | |
| Maximum Acceleration Values, in units of 'g' | | | | | | | | | |
| Payload of 11.5 kg | | | | | Payload of 14.9 kg | | | | |
| | | Amplitude (mVpp) | | | | | Amplitude (mVpp) | | |
| Current (A) | Location | 200 | 400 | 600 | Current (A) | Location | 200 | 400 | 600 |
| 0 | Base | | 0.0951 | | 0 | Base | | | |
| 0 | Payload | | 0.0911 | | 0 | Payload | | | |
| 0.2 | Base | | 0.1073 | | 0.2 | Base | | 0.1373 | |
| 0.2 | Payload | | 0.0970 | | 0.2 | Payload | | 0.0710 | |
| 0.4 | Base | | 0.1190 | | 0.4 | Base | | 0.0894 | |
| 0.4 | Payload | | 0.0931 | | 0.4 | Payload | | 0.0695 | |
| 0.5 | Base | 0.0991 | 0.1593 | 0.1384 | 0.5 | Base | 0.0651 | 0.1796 | |
| 0.5 | Payload | 0.0544 | 0.0959 | 0.1056 | 0.5 | Payload | 0.0677 | 0.0740 | |
| 0.6 | Base | | 0.1857 | | 0.6 | Base | | 0.1310 | |
| 0.6 | Payload | | 0.0974 | | 0.6 | Payload | | 0.0701 | |
| 0.7 | Base | 0.0795 | 0.1855 | 0.1507 | 0.7 | Base | | 0.0830 | |
| 0.7 | Payload | 0.0440 | 0.0990 | 0.1180 | 0.7 | Payload | | 0.0712 | |
| 1 | Base | | | | 1 | Base | | 0.8765 | |
| 1 | Payload | | | | 1 | Payload | | 0.0943 | |
| 1.5 | Base | | | | 1.5 | Base | | 0.1615 | |
| 1.5 | Payload | | | | 1.5 | Payload | | 0.1276 | |

The comparison between the RMS and peak values of acceleration between the base and payload is shown in the form of bar graphs in Figs. 4.27 to 4.32. The RMS acceleration is seen to be mitigated at all current levels in Figures 4.27 and 4.28 with the exception of 0 A. This is because damping is particularly low where there is no current input to the electromagnet of the damper.
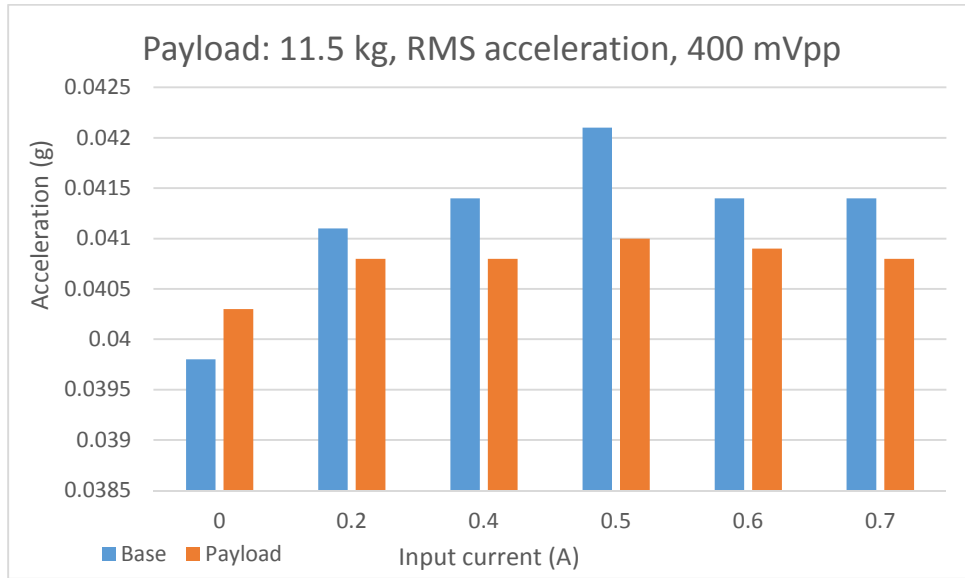


Figure 4.27: Comparison of base and payload RMS values, payload: 11.5 kg, amplitude: 400 mVpp, frequency sweep: 9-16 Hz over 60 seconds.
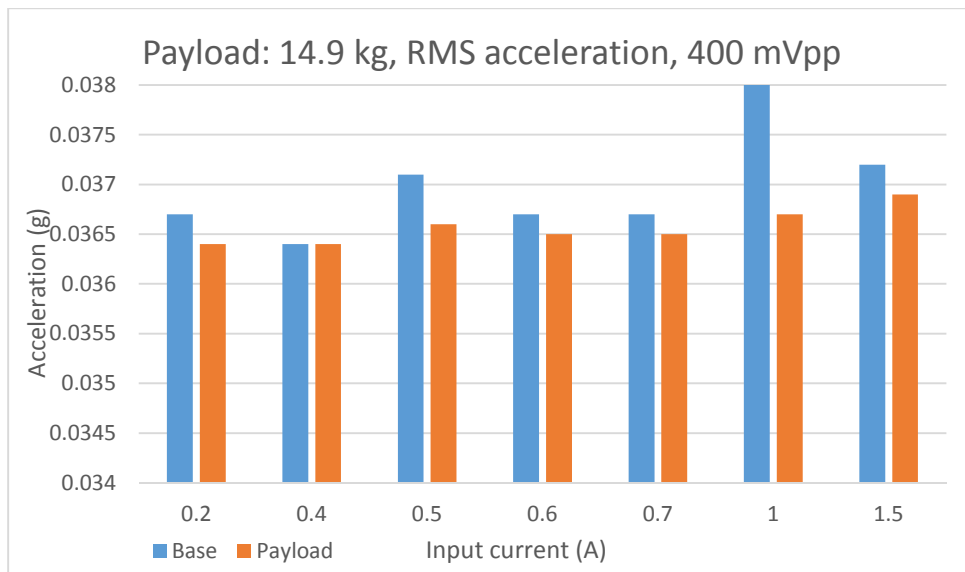


Figure 4.28: Comparison of base and payload RMS values, payload: 14.9 kg, amplitude: 400 mVpp, frequency sweep: 9-16 Hz over 60 seconds.

The mitigation levels are particularly high when the peak values of acceleration are compared, as seen in Figures 4.29 and 4.30. Mitigation is seen to increase to 60% or above when the input current is increased to 0.5A or above. These results are indicative of the semi-active capability of the damper, that is to say that the damper can be adjusted to provide a specific level of vibration isolation.
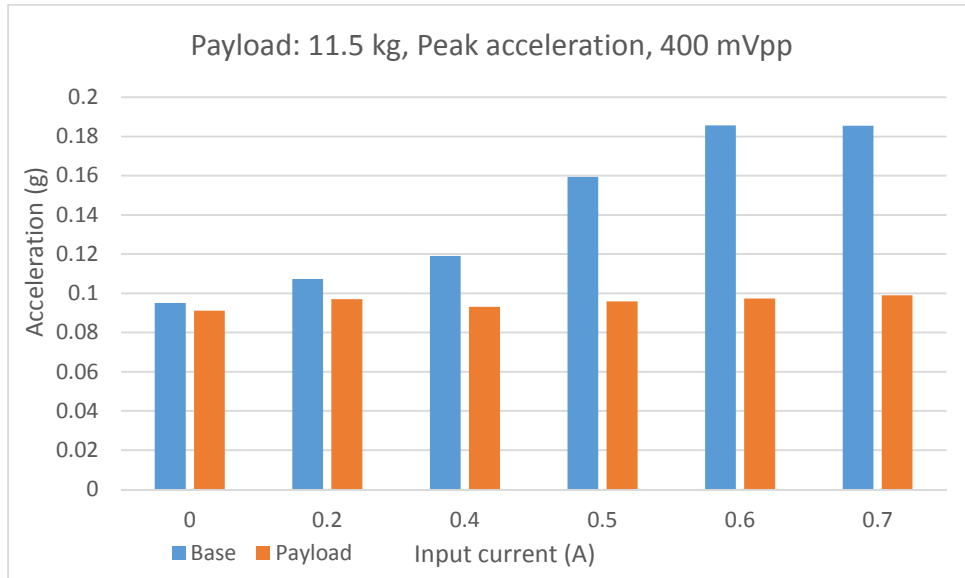


Figure 4.29: Comparison of base and payload peak acceleration values, payload: 11.5 kg, amplitude: 400 mVpp, frequency sweep: 9-16 Hz over 60 seconds.
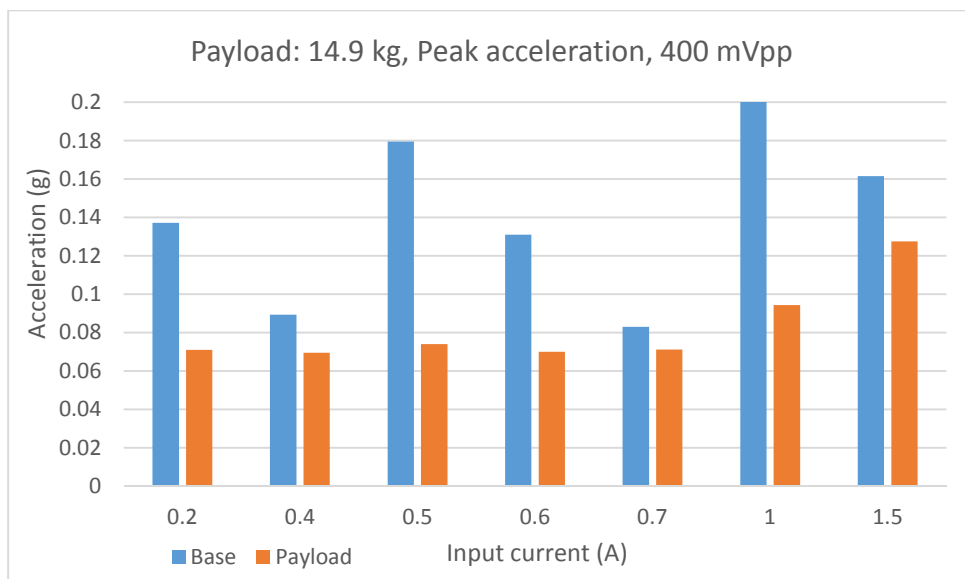


Figure 4.30: Comparison of base and payload peak acceleration values, payload: 14.9 kg, amplitude: 400 mVpp, frequency sweep: 9-16 Hz over 60 seconds.

Figures 4.31 and 4.32 show one more comparison between the acceleration levels of the base and the payload with the changing excitation amplitude. As can be seen from these figures, the mitigation stays high even with increased excitation amplitudes, particularly when the peak levels are compared, as seen in Figure 4.32.
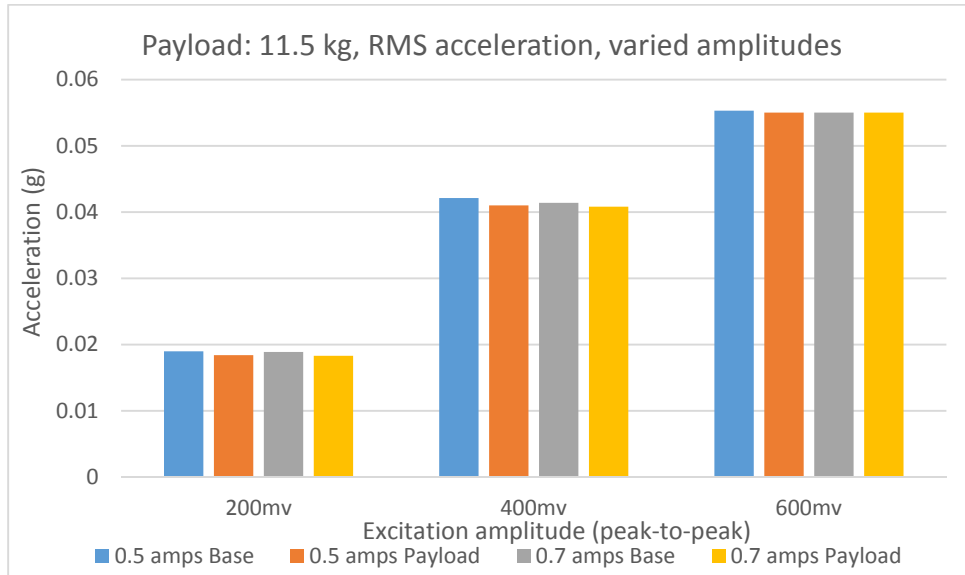


Figure 4.31: Comparison of base and payload RMS acceleration values over various amplitudes of excitation (200, 400, 600mVpp). Frequency sweep: 9-16 Hz over 60 seconds, payload: 11.5 kg.
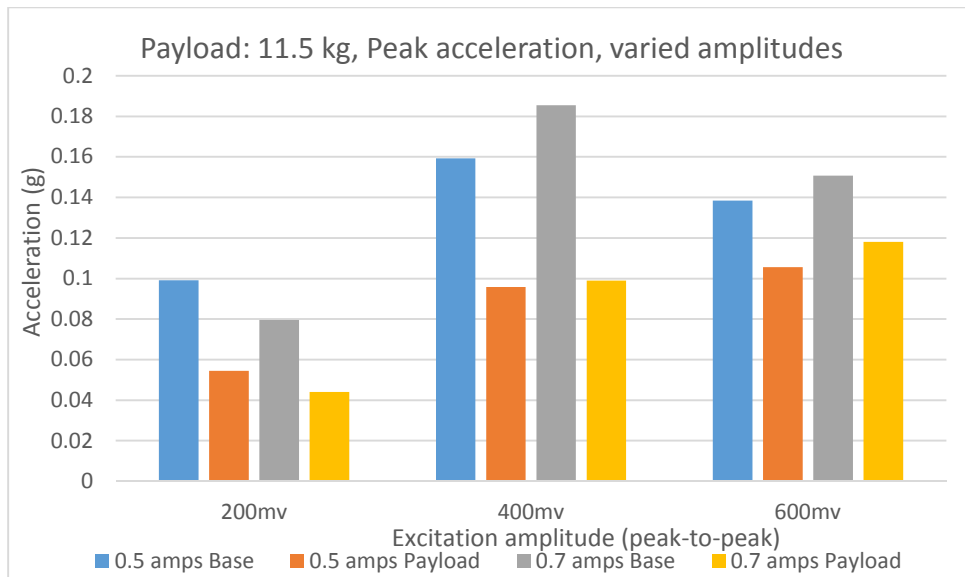


Figure 4.32: Comparison of base and payload peak acceleration values over various amplitudes of excitation (200, 400, 600mVpp). Frequency sweep: 9-16 Hz over 60 seconds, payload: 11.5 kg.

## 4.4. Conclusion

From the test results discussed in this chapter, it can be concluded that the MR damper exhibits characteristics that demonstrate a semi-active behavior. Direct control of input current to the electromagnet of the damper can be used to reduce the force that is transmitted to a payload due to base excitation. The damper is seen to behave consistently with increase in the current resulting in an increase in damping. Peak accelerations were found to be reduced by 50 to 70% in some cases, showcasing the capability of the damper with adjustable current. The damper characterization demonstrates very little change in stiffness. This characterization is used to build the model for calculating transmissibility. The test setup developed for this study is reliable and robust and can be used for future testing.

CHAPTER 5 :   CONCLUSIONS AND FUTURE WORK

While the existing damping technologies are pretty effective and are being widely used in automotive and industrial applications, there is a universal pursuit for improvement in order to enhance ergonomics and increase fatigue life. To this end, active materials are being investigated and utilized more often to overcome limitations and constraints associated with current technologies involving passive damping. The focus of this study has been on one such semi-active material that has shown promise, namely magnetorheological fluid that is used in dampers.

## 5.1.    Research Goals

The primary goal of this research is to gain a clear understanding of a commercial MR damper and its properties and characteristics within a range of test conditions. While these test conditions include several variables at multiple levels, some of the extreme limits of the damper's capabilities have not been investigated in this study due to constraints of the test facilities. Some of these aspects of research limitations are discussed in Section 5.3 as part of possible future scope for this study. The main influences of multiple variables affecting the damper's capability in mitigating vibrations are investigated and presented in this chapter.

## 5.2.    Results and Observations

From the analysis of all the data collected for this study, it can be concluded that the damper behavior is generally seen to be as per expectations of a semi-active damper. There are some exceptions or observations that may be attributed to different reasons or a lack of extensive data. In general, increasing the input current to the electromagnet resulted in an enhancement of vibration mitigation with an increase in the difference between the base and payload accelerations. In many cases, however, the rise in the current level caused a disproportionate increase in the acceleration of the base. This is exemplified from the results in Figure 4.29 in Chapter 4, which shows peak acceleration values for a payload of 11.5 kg. The RMS values for the same data set are seen in Figure 4.27, where somewhat similar results are shown – both base and payload are seemingly affected by a change in current, but the base is seen to be

affected more severely than the payload. The relative increase in the acceleration levels at the base is not proportional to the increase in the acceleration levels of the payload. The underlying reasons for this are not completely understood and will require further investigation.

The stiffness of the damper is seen to remain constant with an increase in the input current while the damping constant increases, as seen in Table 4.2 in Chapter 4. Although the stiffness constant may also increase with the increasing current, this has not been observed in this study since small excitation amplitudes have been used for base excitation. Changes in excitation frequency (within the tested range) do not appear to have a significant effect on vibration mitigation. However, the excitation amplitude is seen to have a direct effect on acceleration levels. In all cases, the input current supplied to the electromagnet of the damper is seen to have a direct influence on transmitted vibration and can be used as the control variable for the damper. The change in input current directly influences the strength of the magnetic field, affecting the fluid's yield strength, as discussed in Chapters 2 and 3. External factors such as the mass of the payload are seen to have a significant influence, as seen in Figures 5.1 and 5.2. Figures 5.1 and 5.2 show the difference between the RMS accelerations of the base and the payload at multiple levels of input current for two different payloads. The acceleration of the base is consistently higher than the acceleration of the payload for all test cases, as seen in Figures 5.1 and 5.2, but there is no apparent trend in the level of mitigation.
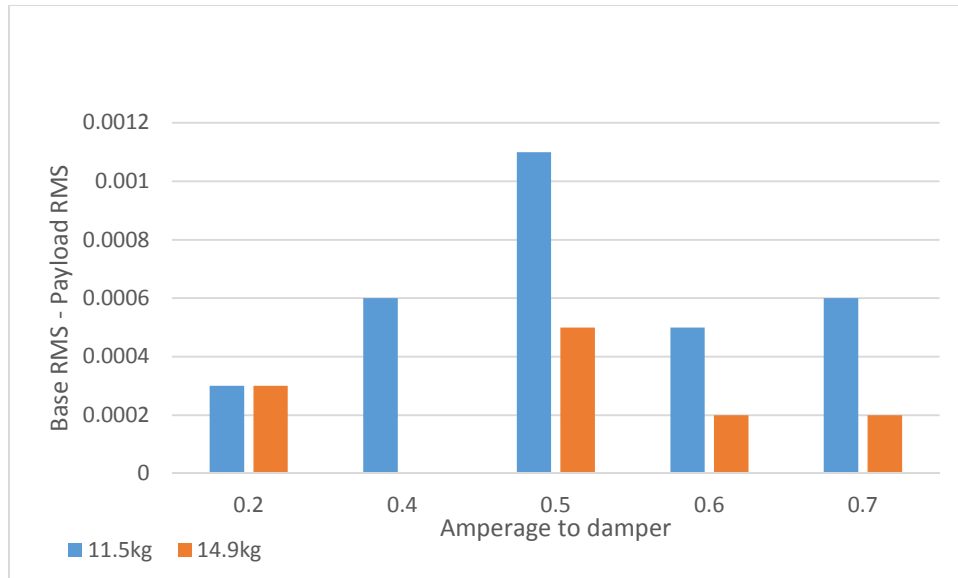
Figure 5.1: Comparison of RMS acceleration between payload and base as a function of payload mass and input current.
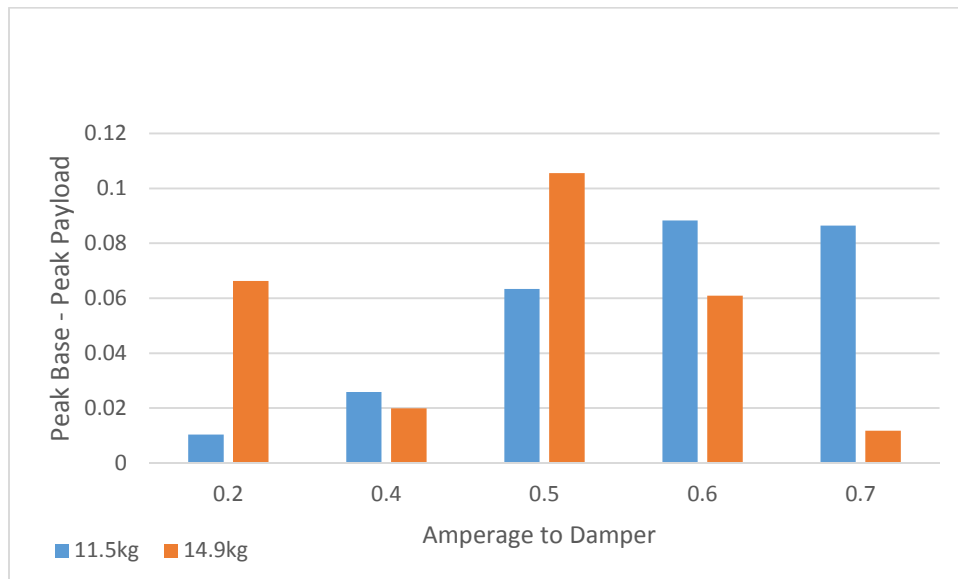


Figure 5.2: Comparison of peak acceleration between payload and base as a function of payload mass and input current.

Figures 5.3 and 5.4 show the effects of excitation amplitude at two different current levels (0.5 A and 0.7 A) and at a constant payload of 11.5 kg. While the RMS acceleration is highest at the excitation

amplitude of 400mV, there is no clear trend within this data. Further data collection may be necessary in order to comprehend this effect.
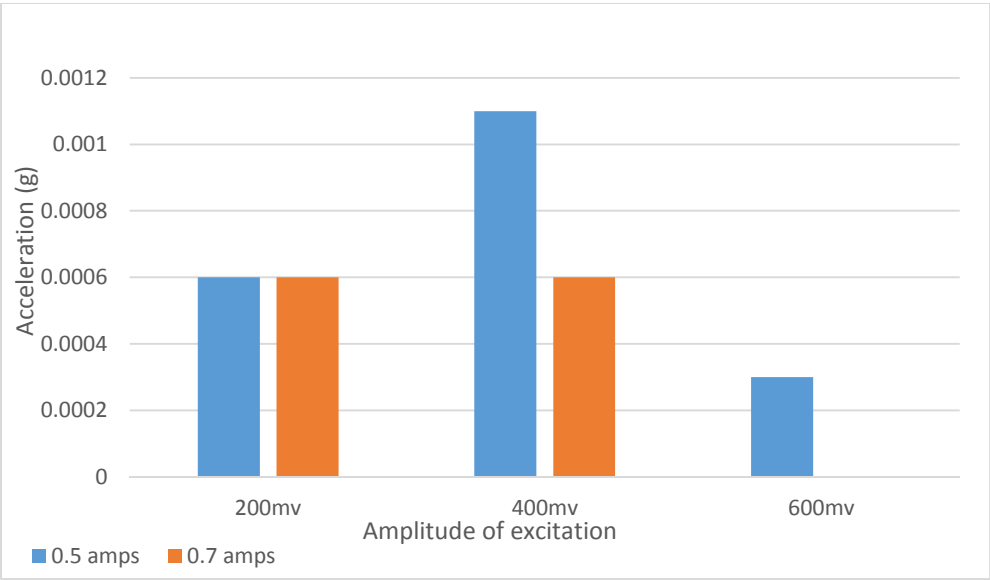


Figure 5.3: RMS acceleration – varying excitation amplitude, 11.5 kg payload.
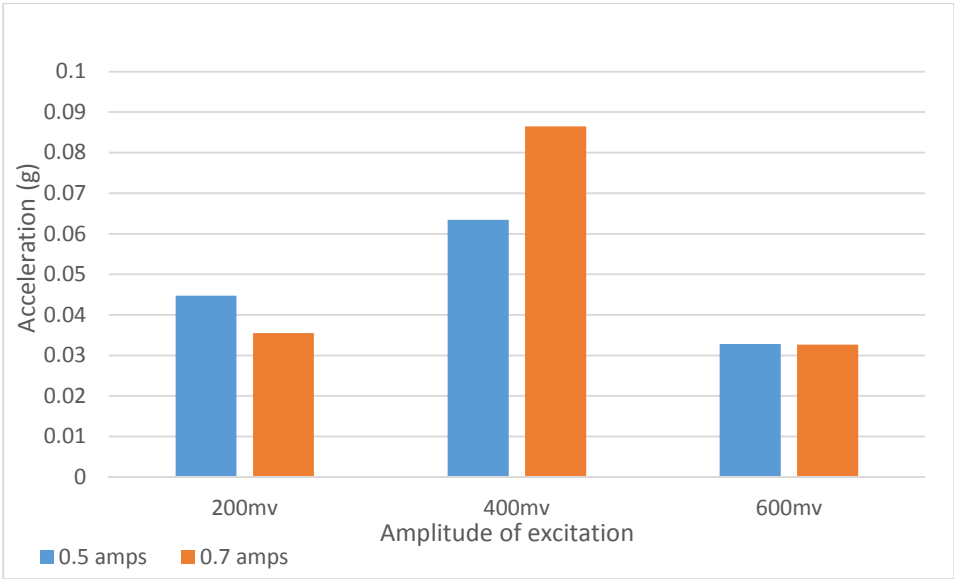


Figure 5.4: Peak acceleration – varying excitation amplitude, 11.5 kg payload.

By comparing the RMS values of the measured accelerations from the base and payload, there is an observable trend of increased vibration mitigation with an increase in input current. This trend is

especially noticeable when comparing the peak acceleration of the base to the payload, as in Figure 4.29, while comparing the peak values at a payload of 11.5 kg. This can be compared to Figure 4.30, where a payload of 14.9 kg is used and the peak accelerations are compared between the base and payload.

For the payload of 11.5 kg, the reduction in the maximum acceleration ranges from 4.2% to 47.5%. However, input current above 1 A increases the maximum acceleration. This is possibly due to a significant increase in damping and can be corroborated from the transmissibility plots discussed in Chapter 3. The comparison of RMS acceleration shows a mitigation ranging from 0.75% to 2.6%. This is relatively lower than the comparison of the maximum acceleration levels since the RMS value represents the entire time history and because base excitation is provided from 9 to 16 Hz. Similar results have been reported in the literature for shock isolation through MR dampers. For a payload of 14.9 kg, a 29% increase over the payload of 11.5 kg, the mitigation results range from 4.7% to 39.8% while comparing the RMS and the maximum values of acceleration between the payload and the base. These levels of mitigation are comparable to the performance with the lower payload. This test serves as a validation of the capability of the MR damper in dealing with variable payloads due to its inherent ability to adjust damping levels.

It can be concluded that the experimental setup and the test method developed for this study are robust and can be replicated for a similar study of vibration mitigation. The setup also allows for easy and efficient changes of payload, as well as the simple adjustments to the excitation levels and input current to the damper. The influence of variables such as payload mass, excitation amplitude and excitation frequency has been successfully assessed through the setup designed for this study. It is found that the damper is robust and is capable of handling payload and excitation variability. The semi-active nature of the MR damper is a key attribute, meaning that the damper continues to be functional even if the control circuit and the electromagnet fail.

With regards to the data collected from this study, it may be necessary to investigate other measures of quantification of acceleration over a large period in time. While the RMS values of acceleration are convenient and provide one value, they may not adequately represent the results. The

peak values of acceleration are convenient to use but they only represent one value of acceleration in the entire time history and could, therefore, be misleading. The choice of the appropriate range of excitation frequency is important in any vibration testing. In this study, the range of excitation frequency has been selected to be well above the natural frequency (around 1 Hz) in order to evaluate vibration mitigation at high frequency ratios (9 and above). However, this may not capture the needs of some systems and needs to be evaluated carefully on a case-by-case basis.

### 5.3. Future Work

There are several directions that the future work with the MR damper could take. A direct continuation of this research would be to simply continue collecting data at multiple additional settings in order to verify the repeatability of the data presented, and to statistically determine any trends that may be present. An important aspect of this line of continuation would be to use excitation frequency as a factor at multiple levels instead of using a frequency sweep. This would significantly increase the amount of data collection, but could provide more insight into the capability of the damper. There is a significant difference between the peak and RMS values of acceleration, as expected. It may be worth investigating a more consistent method of simplifying and reporting the acceleration values, or modifying the test method for that purpose. This modification may in fact be necessary to run a statistical analysis on the various input factors.

Future work could involve the investigation of a control algorithm for the damper. This could potentially quantify the outputs from properly placed accelerometers and adjust the current to the damper accordingly, resulting in an actively adjusting damping system in a closed loop. Current literature outlines various control schemes and methods but the control algorithms are non-trivial since the damping level is not directly controlled and is dependent on multiple variables. The experimental setup developed in this study can be used for this purpose.

Other future work can include a continued investigation into the damper's capabilities with further investigation under a broader range of frequencies, for instance between 10 and 500 Hz with multiple higher payloads. This study could include higher displacement amplitudes, but that would

require another shaker table. The use of a shock dynamometer would allow testing the damper at higher displacements amplitudes (at the expense of higher frequencies), this could greatly expand the scope of the research. Other areas of work could include an investigation of environmental effects such as temperature. It is known that the MR damper exhibits a strong temperature dependent behavior. An investigation of the damper's performance across a broad range of temperatures would be useful for any real-life application of the damper. Durability and fatigue testing of the damper at multiple duty cycles could provide valuable information during the selection process of a suitable damper. During the course of this study, the damper was never excited continuously for more than ten minutes at a given time. This limited usage does not represent the needs of an application that may involve more than a million cycles of operation. The use of the damper can also be investigated for specific applications. One such study is being currently undertaken by a fellow graduate student in our research group that involves the use of MR dampers in a motorcycle suspension system.

# WORKS CITED

[1] Olabi, A.G., Grunwald, A., 2007, Design and application of a magneto-rheological fluid, Materials and Design, Vol. 28, pp. 2658-2664.

[2] Zhang, X., Li, W., Gong, X.L., 2008, Study on magnetorheological shear thickening fluid, Smart Materials and Structures, Vol. 17, pp. 015051-1-6.

[3] Choi, S., Seong, M., Ha, S., 2009, Vibration control of an MR vehicle suspension system considering both hysteretic behavior and parameter variation, Smart Materials and Structures, Vol. 18, pp. 125010-1-14.

[4] Carlson, J.D., Jolly, M.R., 2000, MR fluid, foam, and elastomer devices, Mechatronics, Vol. 10, pp. 555-569.

[5] Namuduri, C.S., Golden, M.A., Praeckel, J., 2003, Concurrent research and development of a magnetic ride control system, Industrial Electronics Society, IECON '03, The 29th Annual Conference of the IEEE, Vol. 3, pp. 2853-2858.

[6] Wilson, T. (n.d.), Retrieved June 10, 2015, from http://science.howstuffworks.com/liquid-body-armor2.htm.

[7] Ikhouane, F., Dyke, S.J., 2007, Modeling and identification of a shear mode magnetorheological damper, Smart Materials and Structures, Vol. 16, pp. 605-616.

[8] Kaul, S., 2011, Recursive modeling of a magnetorheological damper, International Journal of Mechanical and Materials Engineering (IJMME), Vol. 6, pp. 31-40.

[9] Strydom, A., Kaul, S., Els, P.S., 2012, Magneto-rheological (MR) Damper Modeling for Semi-active Control without Force Feedback, ASME-IDETC, DETC2012-70311, Chicago, IL.

[10] Dong, X., Yu, M., Liao, C., Chen, W., 2010, Comparative research on semi-active control strategies for magneto-rheological suspension, Nonlinear Dynamics, Vol. 59, pp. 433-453.

[11] Sarigul-Klijn, N., Lopez, I., Sarigul-Klijn, M., Karnopp, D., 2007, Vibration mitigation using passive active tunable (PAT) system: Experimental aspects, Journal of Vibration and Acoustics, Vol. 129, pp. 209-216.

[12] Ahmadian, M., Pare, C.A., 2000, A quarter-car experimental analysis of alternative semiactive control methods, Journal of Intelligent Material Systems and Structures, Vol. 11, pp. 604-609.

[13] Yu, M., Liao, C.R., Chen, W.M., Huang, S.L., 2006, Study on MR semi-active suspension system and its road testing, Journal of Intelligent Material Systems and Structures, Vol. 17, pp. 801-806.

[14] Liu, C.X., Liu, X.H., Gao, X.L., Yu, H., Lin, G.W., 2015, Mechanics Performance of a Novel Magneto-Rheological Fluid Damper, Journal of Testing and Evaluation, Vol. 43, DOI: 10.1520/JTE20140133.

[15] Choi, Y-T., Wereley, N.M., 2008, Shock Isolation Systems Using Magnetorheological Dampers, Journal of Vibration and Acoustics, Vol. 130, pp. 024503-1-6.

All the MATLAB programs developed and used for this study are provided in Appendix A.

The following MATLAB program provides an example of the post-processing and analysis that has been performed after collecting the accelerometer data.

```matlab
% Data - description of data set
aa=xlsread('name of excel file');

aa_base=aa(:,2)/10; %column 2 in the excel file is channel 0, base
%[B,A] = butter(6,50/800,'low');
[B,A] = butter(6,[5/800 140/800]);
%h = fvtool(B,A);
a_base=filter(B,A,aa_base);
rms_base_static=norm(a_base)/sqrt(length(a_base)-1)
max_base_static=max(abs(a_base))

aa_payload=aa(:,3)/10; %column 3 in the excel file is channel 1, payload
%[B,A] = butter(6,50/800,'low');
[B,A] = butter(6,[5/800 140/800]);
a_payload=filter(B,A,aa_payload);
rms_payload_static=norm(a_payload)/sqrt(length(a_payload)-1)
max_payload_static=max(abs(a_payload))

figure,plot(aa(:,1),abs(a_base),'g',aa(:,1),abs(a_payload),'r'),grid
legend('Table','Payload'),xlabel('Time (s)'), ylabel('Acceleration (g)')
title('Title of plot')  %
xlim([5 100])

Fs=1600;
L=length(a_base);
y_b=a_base;
NFFT=2^nextpow2(L);
y_bf=fft(y_b,NFFT)/L;
f_b=Fs/2*linspace(0,1,NFFT/2+1);
% rms_bf=norm(y_bf)/sqrt(length(y_bf)-1)

L=length(a_payload);
y_p=a_payload;
NFFT=2^nextpow2(L);
y_pf=fft(y_p,NFFT)/L;
f_p=Fs/2*linspace(0,1,NFFT/2+1);
% rms_pf=norm(y_pf)/sqrt(length(y_pf)-1)

figure,semilogx(f_b,2*abs(y_bf(1:NFFT/2+1)),'g') % plots frerquency response,
x-axis is a logarithmic scale
hold on
semilogx(f_p,2*abs(y_pf(1:NFFT/2+1)),'r'),grid
```

```matlab
legend('Table','Payload'),xlabel('Frequency (Hz)'),ylabel('Frequency
Response')
%xlim([1 100])
title('title of plot')

figure,plot(f_b,2*abs(y_bf(1:NFFT/2+1)),'g') % plots frerquency response, x-
axis is a linear scale
hold on
plot(f_p,2*abs(y_pf(1:NFFT/2+1)),'r'),grid
legend('Table','Payload'),xlabel('Frequency (Hz)'),ylabel('Frequency
Response')
title('title of plot')

%figure, plot(f_p,(abs(y_pf(1:NFFT/2+1))./abs(y_bf(1:NFFT/2+1)))'),grid
%figure, semilogx(f_p,(abs(y_pf(1:NFFT/2+1))./abs(y_bf(1:NFFT/2+1)))'),grid

% Transmissibility
% Ta=a_payload./a_base;
% Fs=1600;
% L=length(Ta);
% NFFT=2^nextpow2(L);
% Taf=fft(Ta,NFFT)/L;
% Taff=Fs/2*linspace(0,1,NFFT/2+1);
% figure, semilogx(Taff,2*abs(Taf(1:NFFT/2+1))),grid
% xlim([5 100])
% xlabel('Frequency (Hz)'),ylabel('Acceleration Transmissibility')

figure, scatter(a_base,a_payload),grid % scatter plot of acceleration values
xlim([-0.2 0.2]),ylim([-0.2 0.2])
xlabel('Table acceleration (g)'),ylabel('Payload acceleration (g)')
title('title of plot')
```

The following MATLAB program has been used to generate Figures 3.3 and 3.4, the theoretical models for force and displacement transmissibility for the MR damper at various current levels.

```matlab
% Transmissibility

m=10;%kg
k=0.1*1000;% N/m
c=0;
zeta=c/(2*sqrt(m*k));
wn=sqrt(k/m);

T=[];Tf=[];

for r=0:0.1:15;
    t=sqrt((1+(2*zeta*r)^2)/((1-r^2)^2+(2*zeta*r)^2));
    tf=r^2*t;
    T=[T t];Tf=[Tf tf];
end
figure, plot(0:0.1:15,T,'--rs','LineWidth',2),grid
hold on

k=0.1*1000;% N/m
c=2.5;%N-s/m

zeta=c/(2*sqrt(m*k));
wn=sqrt(k/m);

T0=[];T0f=[];

for r=0:0.1:15;
    t=sqrt((1+(2*zeta*r)^2)/((1-r^2)^2+(2*zeta*r)^2));
    t0f=r^2*t;
    T0=[T0 t];T0f=[T0f t0f];
end
plot(0:0.1:15,T0,'-b','LineWidth',2)
hold on

k=0.15*1000;% N/m
c=20;%N-s/m

zeta=c/(2*sqrt(m*k));
wn=sqrt(k/m);

T0_5=[];T0_5f=[];

for r=0:0.1:15;
    t=sqrt((1+(2*zeta*r)^2)/((1-r^2)^2+(2*zeta*r)^2));
    t0_5f=r^2*t;
    T0_5=[T0_5 t];T0_5f=[T0_5f t0_5f];
end
plot(0:0.1:15,T0_5,'c','LineWidth',2)
hold on
```

```matlab
k=0.15*1000;% N/m
c=30;%N-s/m

zeta=c/(2*sqrt(m*k));
wn=sqrt(k/m);

T1=[];T1f=[];

for r=0:0.1:15;
    t=sqrt((1+(2*zeta*r)^2)/((1-r^2)^2+(2*zeta*r)^2));
    t1f=r^2*t;
    T1=[T1 t];T1f=[T1f t1f];
end
plot(0:0.1:15,T1,'-.k','LineWidth',2)
hold on

k=0.15*1000;% N/m
c=37.5;%N-s/m

zeta=c/(2*sqrt(m*k));
wn=sqrt(k/m);

T1_5=[];T1_5f=[];

for r=0:0.1:15;
    t=sqrt((1+(2*zeta*r)^2)/((1-r^2)^2+(2*zeta*r)^2));
    t1_5f=r^2*t;
    T1_5=[T1_5 t];T1_5f=[T1_5f t1_5f];
end
plot(0:0.1:15,T1_5,'-*g','LineWidth',2),ylim([0 3]),xlim([0 5])
legend('Undamped','0A','0.5A','1A','1.5A'),xlabel('Frequency ratio
\omega/\omega_n'),ylabel('T_d'),title('Displacement Transmissibility')

figure,plot(0:0.1:15,T0,'-b',0:0.1:15,T0_5,'c',0:0.1:15,T1,'-
.k',0:0.1:15,T1_5,'-*g','LineWidth',2),grid
ylim([0 3]),xlim([0 5])
legend('0A','0.5A','1A','1.5A'),xlabel('Frequency ratio
\omega/\omega_n'),ylabel('T_d'),title('Displacement Transmissibility')

figure,plot(0:0.1:15,Tf,'--rs',0:0.1:15,T0f,'-
b',0:0.1:15,T0_5f,'c',0:0.1:15,T1f,'-.k',0:0.1:15,T1_5f,'-
*g','LineWidth',2),grid
ylim([0 3]),xlim([0 5])
legend('Undamped','0A','0.5A','1A','1.5A'),xlabel('Frequency ratio
\omega/\omega_n'),ylabel('T_f'),title('Force Transmissibility')
```

The following MATLAB program has been used to analyze and plot the data collected from the tensile testing, and subsequently used to characterize the damper.

```matlab
data_1 = xlsread('Data_1');
t1 = data_1(:,1); % time in seconds
x1 = data_1(:,2); % displacement in mm
xdot1=diff(x1)/0.1;
xdot1=[0; xdot1];
f1 = data_1(:,3); % force in N (also called kgf)

figure, plot(x1,f1),grid,ylim([0 20])
xlabel('Displacement (mm)'), ylabel('Force (N)')
title('Damper Characteristics - 0A')
figure, scatter(xdot1,f1),grid
xlabel('Velocity (mm/s)'), ylabel('Force (N)')
title('Damper Characteristics - 0A')

data_2 = xlsread('Data_2');
t2 = data_2(:,1); % time in seconds
x2 = data_2(:,2); % displacement in mm
xdot2=diff(x2)/0.1;
xdot2=[0; xdot2];
f2 = data_2(:,3); % force in N

figure, plot(x2,f2),grid,ylim([0 20])
xlabel('Displacement (mm)'), ylabel('Force (N)')
title('Damper Characteristics - 0.5A')
figure, scatter(xdot2,f2),grid
xlabel('Velocity (mm/s)'), ylabel('Force (N)')
title('Damper Characteristics - 0.5A')

data_3 = xlsread('Data_3');
t3 = data_3(:,1); % time in seconds
x3 = data_3(:,2); % displacement in mm
xdot3=diff(x3)/0.1;
xdot3=[0; xdot3];
f3 = data_3(:,3); % force in N

figure, plot(x3,f3),grid,ylim([0 20])
xlabel('Displacement (mm)'), ylabel('Force (N)')
title('Damper Characteristics - 1.5A')
figure, scatter(xdot3,f3),grid
xlabel('Velocity (mm/s)'), ylabel('Force (N)')
title('Damper Characteristics - 1.5A')


data_4 = xlsread('Data_4');
t4 = data_4(:,1); % time in seconds
x4 = data_4(:,2); % displacement in mm
xdot4=diff(x4)/0.1;
xdot4=[0; xdot4];
f4 = data_4(:,3); % force in N
```

```matlab
figure, plot(x4,f4),grid,ylim([0 20])
xlabel('Displacement (mm)'), ylabel('Force (N)')
title('Damper Characteristics - 1A')
figure, scatter(xdot4,f4),grid
xlabel('Velocity (mm/s)'), ylabel('Force (N)')
title('Damper Characteristics - 1A')

figure,plot(x1,f1,x2,f2,x4,f4,x3,f3,'LineWidth',2),grid,ylim([0 20])
legend('0A','0.5A','1A','1.5A')
xlabel('Displacement (mm)'), ylabel('Force (N)')
title('Damper Characteristics')
```

APPENDIX B: SPECIFICATIONS AND DATA SHEETS

Appendix B provides the specification sheets for the main equipment used during this research. The specification sheets for the damper, the controller kit, the power amplifier, the accelerometer and the shaker table are included for reference.

# RD-8040-1 and RD-8041-1 Dampers

## Description

LORD RD-8040-1 (short stroke) and RD-8041-1 (long stroke) dampers are compact, magneto-rheological (MR) fluid dampers suitable for industrial suspension applications. Continuously variable damping is controlled by the increase in yield strength of the MR fluid in response to magnetic field strength.

## Features and Benefits

*Fast Response Time* – responds in less than 15 milliseconds to changes in the magnetic field.

*Easy to Use* – provides simple electronics and straight forward controls.

*Durable* – provides excellent long term stability.

## Storage

Dampers should be stored at -40 to +100°C (-40 to +212°F).

The RD-8040-1 and RD-8041-1 dampers are monotube shocks containing high-pressure nitrogen gas (300 psi). Handle with care and do not heat or puncture body.

## Electrical Properties*

| | |
|---|---|
| Input Current, Amp | |
| Continuous for 30 seconds | 1 max |
| Intermittent | 2 max |
| Input Voltage, Volt | 12 DC |
| Resistance, ohms | |
| @ ambient temperature | 5 |
| @ 71°C (160°F) | 7 |

*Data is typical and not to be used for specification purposes.

## Typical Properties*

| | RD-8040-1 | RD-8041-1 |
|---|---|---|
| Stroke, mm (in) | 55 (2.17) | 74 (2.91) |
| Extended Length, mm (in) | 208 (8.2) | 248 (9.76) |
| Body Diameter, mm (in) | 42.1 (1.66) max | 42.1 (1.66) max |
| Shaft Diameter, mm (in) | 10 (0.39) | 10 (0.39) |
| Tensile Strength, N (lbf) | 8896 (2000) max | 8896 (2000) max |
| Damper Forces, N (lbf) Peak to Peak | | |
| 5 cm/sec @ 1 A | >2447 (>550) | >2447 (>550) |
| 20 cm/sec @ 0 A | <667 (<150) | <667 (<150) |
| Operating Temperature, °C (°F) | 71 (160) max | 71 (160) max |

*Data is typical and not to be used for specification purposes.

## LORD
### AskUsHow™

**Typical Force vs. Velocity**



Velocity (m/sec)
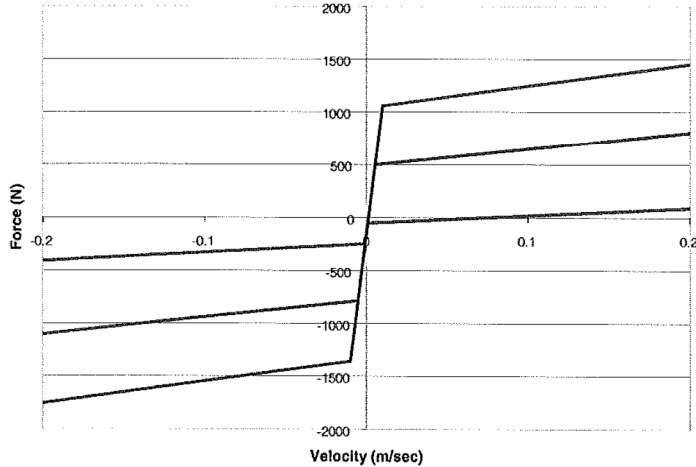
*Offset at origin is due to gas precharge required for temperature compensation and to prevent cavitation.*

Values stated in this technical data sheet represent typical values as not all tests are run on each lot of material produced. For formalized product specifications for specific product end uses, contact the Customer Support Center.

Information provided herein is based upon tests believed to be reliable. In as much as LORD Corporation has no control over the manner in which others may use this information, it does not guarantee the results to be obtained. In addition, LORD Corporation does not guarantee the performance of the product or the results obtained from the use of the product or this information where the product has been repackaged by any third party, including but not limited to any product end-user. Nor does the company make any express or implied warranty of merchantability or fitness for a particular purpose concerning the effects or results of such use.

"Ask Us How" is a trademark of LORD Corporation or one of its subsidiaries.

LORD provides valuable expertise in adhesives and coatings, vibration and motion control, and magnetically responsive technologies. Our people work in collaboration with our customers to help them increase the value of their products. Innovative and responsive in an ever-changing marketplace, we are focused on providing solutions for our customers worldwide ... Ask Us How.

**LORD**
AskUsHow™

| REV | DESCRIPTION | DATE | DR |
|---|---|---|---|
| A | PCN RD-1005-3-A | 10/24/2011 | JK |
| B | PCN RD-1005-3-B | 1/20/2006 | SL |

NOTES:

1. ALL DIMENSIONS ARE REFERENCE DIMENSIONS.

2. FOR INSTALLATION ON 12mm SHAFT.

3. ELECTRICAL SPECIFICATIONS:
   INPUT CURRENT
   = 1 AMP MAX. CONTINUOUS
   = 2 AMPS MAX. INTERMITTENT
   INPUT VOLTAGE = 12VDC
   RESISTANCE = 5 Ω AT AMBIENT TEMPERATURE
   RESISTANCE = 7 Ω AT 71°C (160°F)

4. DAMPER FORCE: (PEAK TO PEAK)
   0.05 M/S AT 1 AMP = > 2224 N (500 POUNDS)
   0.20 M/S AT 0 AMP = < 667 N (150 POUNDS)

5. MECHANICAL SPECIFICATIONS:
   MAXIMUM TENSILE LOAD = 4448 N (1000 POUNDS)
   MAXIMUM OPERATING TEMPERATURE = 71°C (160°F)
   STORAGE TEMPERATURE LIMITS: = -40°C TO 100°C (-40°F TO 212°F)

6. DURABILITY
   DAMPER FORCE (PEAK TO PEAK) @ 0.20 M/S @ 0 AMPS = < 890 N (200 POUNDS).
   AFTER 2 MILLION CYCLES @ +/- 12.5mm, 2 HERTZ WITH INPUT CURRENT VARYING
   BETWEEN 0 AND 0.8 AMPS.

7. DESIGN NOTE:
   DAMPER STROKE MUST BE LIMITED WITHIN THE SPECIFIED STROKE RANGE. ALLOW A
   MINIMUM SAFETY CLEARANCE OF 6mm OR DAMPER DAMAGE MAY RESULT.

DRAWING RELEASE TYPE   UNLESS OTHERWISE SPECIFIED:

| EXPERIMENTAL | - |
| PROTOTYPE | - |
| PRODUCTION | X |
| FINAL ASSY | |

WEIGHT:
REF. DWG

**LORD**
Materials Division
406 Gregson Dr.
Cary, N. C. 27511-7700

DR. S. M. LAND   1/20/2006

MR DAMPER ASSY.
COMMERCIAL SPEC.

SIZE B   DWG. NO. RD-1005-3   REV B

Sht 1 of 1

2 - 22AWG
15 REF.
20.0 REF.
Ø12.2 REF.
Ø22.2 REF.
100.0 REF.
Ø41.4 REF.
114.0 REF.
EXTENDED LENGTH 209
COMPRESSED LENGTH 155
SEE NOTE 7

# LORD Wonder Box® Device Controller Kit

LORD Wonder Box® device controller kit is a companion product for the magneto-rheological (MR) fluid devices. The kit includes the device controller, 12 Volt DC power supply and two banana plugs.

The Wonder Box device controller kit provides closed loop current control to compensate for changing electrical loads up to the limits of the power supply. The Wonder Box controller may be operated as an interface device for PLC or computer control of MR fluid devices. The Wonder Box device controller kit is for indoor use only.

If manual operation is desired, a potentiometer is provided to control the current supplied to an attached device.

## Operating Instructions

Connect the banana plugs to each wire of the MR fluid device. Insert the banana plugs into the Wonder Box controller output (B). Polarity is not important. Connect the power supply to the input connector (A). The red LED should light indicating proper operation of the unit.

### Manual Control

Current to the device is adjusted by rotating the potentiometer (C) in the clockwise direction. An external voltage control input should not be connected to the BNC terminal (D).

### External Voltage Control

With the potentiometer control set to zero (rotate fully counter clockwise), connect a 0-5 Volt DC control signal to the BNC terminal on the side of the Wonder Box controller (D). Output current to a device can now be controlled with this input signal. The input control signal can be switched up to 1 kHz.

The output current is linearly proportional to the input voltage. The output current will be 0.0 Amps when the control input is approximately 0.4-0.6 Volts at the BNC terminal (refer to Typical Performance graph).

### Pulse Control

In Manual or External Voltage Control, current to the device may be switched on and off by depressing the switch on the side of the controller (E).

## Technical Data

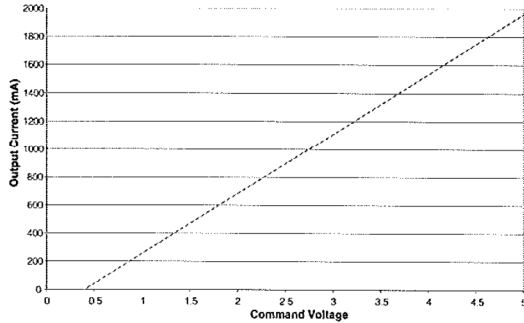| | |
|---|---|
| Overall Dimensions (LxWxH), mm (in) | 63.5 x 27.9 x 88.9 |
| | (2.5 x 1.1 x 3.5) |
| Input Receptacle | 2.1 mm Female |
| Pulse Width Modulation (PWM) Frequency, kHz | 30 |
| Output Current, Amp | 2 max |



*Wonder Box Device Controller*
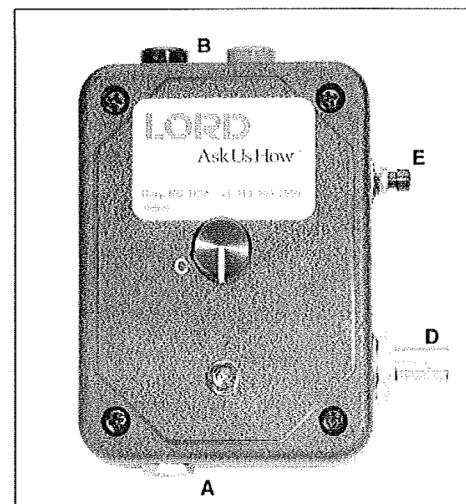
**LORD**
AskUsHow™

### Typical Performance, 4 ohm load



*Performance graph should not be used for control or design purposes.*

The tables below indicate typical performance using the supplied power supply. When utilizing the Wonder Box device controller kit in a control circuit, it is recommended that the user measure the exact voltage to current relationship in their application.

| Input Voltage | Output Current (4 ohm) |
|---|---|
| ~ 0.4-0.6 V | 0 mA |
| 2 V | 750 mA |
| 4.3 V | 1800 mA |

| Input Voltage | Output Current (8 ohm) |
|---|---|
| ~ 0.4-0.6 V | 0 mA |
| 1.6 V | 600 mA |
| 3.2 V | 1300 mA |

Values stated in these instructions represent typical values as not all tests are run on each lot of material produced. For formalized product specifications for specific product end uses, contact the Customer Support Center.

Information provided herein is based upon tests believed to be reliable. In as much as LORD Corporation has no control over the manner in which others may use this information, it does not guarantee the results to be obtained. In addition, LORD Corporation does not guarantee the performance of the product or the results obtained from the use of the product or this information where the product has been repackaged by any third party, including but not limited to any product end-user. Nor does the company make any express or implied warranty of merchantability or fitness for a particular purpose concerning the effects or results of such use.

Wonder Box and "Ask Us How" are trademarks of LORD Corporation or one of its subsidiaries.

LORD provides valuable expertise in adhesives and coatings, vibration and motion control, and magnetically responsive technologies. Our people work in collaboration with our customers to help them increase the value of their products. Innovative and responsive in an ever-changing marketplace, we are focused on providing solutions for our customers worldwide . . . Ask Us How.

**LORD**
AskUsHow™

**Dynamic Transducers and Systems**
21592 Marilla St. • Chatsworth, CA 91311 • Phone 818-700-7818
www.dytran.com • e-mail: info@dytran.com

## OPERATING GUIDE

## MODELS 3019A & 3019A1

## RUGGEDIZED MINIATURE HIGH FREQUENCY

## LIVM™ ACCELEROMETERS,

## HERMETICALLY SEALED

**NOTE:**
MODEL 3019A IS A MINIATURE HIGH FREQUENCY LOW IMPEDANCE
VOLTAGE MODE (LIVM) ACCELEROMETER. IT FEATURES 10 mV/G
SENSITIVITY AND HERMETIC SEALING WITH AN INTEGRAL 1/4-28
MOUNTING STUD AND TOP-MOUNTED 10-32 CONNECTOR. MODEL
3019A1 IS IDENTICAL TO 3019A EXCEPT THE A1 HAS A 10-32
MOUNTING STUD IN PLACE OF THE 1/4-28 STUD ON THE 3019A. ALL
OTHER SPECS. ARE IDENTICAL

**THIS MANUAL INCLUDES:**

1) OPERATING GUIDE, MODEL 3019A & 3019A1
2) OUTLINE/INSTALLATION DWGS., 127-3019A & 127-3019A1
3) SPECIFICATION, MODEL 3019A & 3019A1
4) ARTICLE, "LOW IMPEDANCE VOLTAGE MODE (LIVM) THEORY AND
   OPERATION".

*NOTE: LIVM is Dytran's trademark for its line of Low Impedance Voltage Mode sensors with built-in amplifiers operating
from constant current sources over two wires. LIVM instruments are compatible with other comparable systems
designated as IEPE.

## OPERATING INSTRUCTIONS

### MODELS 3019A & 3019A1 HIGH FREQUENCY LIVM ACCELEROMETERS

### INTRODUCTION

**Model 3019A has a 1/4-28 integral mounting stud. Model 3019A1 has a 10-32 integral stud. All other specifications are similar.**

Series 3019A are miniature high frequency quartz accelerometers with built in impedance converting amplifier. These versatile instruments utilize pure Alfa quartz crystals in compression mode to generate voltage signals exactly analogous to input accelerations including shock and vibration.

An internal MOSFET integrated circuit (IC) amplifier operating as a source follower, converts the very high impedance level signals from the quartz crystals to a low impedance voltage mode signal which is able to drive long cables and feed directly into many types of readout instruments. Output signals are directly in units of mV/g.

The miniature on-board amplifier requires 2 to 20 mA of constant current supplied by special LIVM power units with compliance voltages from +18 to +30 Volts DC. Sensor power and signal are conducted over a single pair of wires allowing the use of inexpensive coaxial cable for system interconnections. Even less expensive twin lead cable may also be used.

Voltage mode systems such as described here feature fixed sensitivity signals, unaffected by cable length. A calibration certificate, traceable to NIST is provided to define the exact sensitivity and frequency response of each instrument.

The sensitivity of Series 3019A is 10.0 mV/g, ± 5% @ 100 Hz and the frequency response is ± 5% from 1 Hz to 10 kHz.

Series 3019A features ground isolated construction, i.e., the mounting surface is electrically isolated from the case (electrical ground) of the instrument. This means that if the test surface is at an elevated electrical potential from power ground, this will have no effect on the sensor signal. This feature precludes annoying "Ground Loops".

Series 3019A are truly hermetically sealed instruments. All joints are TIG welded and the connector is a glass to metal hermetic sealed design.

### DESCRIPTION

Refer to Fig. 1 and Outline/Installation drawings 127-3019A & 127-3019A1)

Both models utilize an upright, compression mode quartz element to maximize the mechanical coupling from mounting base to quartz seismic element for best high frequency fidelity. A special strain isolation base minimizes the unwanted effects of base strain on the accelerometer signal. By careful design and fabrication techniques, the excellent high frequency response and low base strain are optimized.
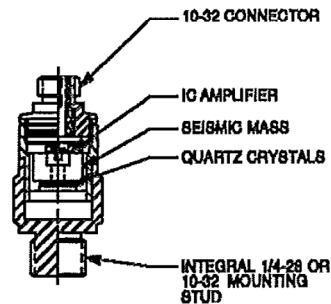


**Figure 1 Cross section series 3019A**

The highly preloaded quartz crystals coupled to a dense tungsten seismic mass ensure excellent linearity over the entire dynamic range with minimal distortion.

The integral MOSFET IC amplifier has been proven dependable to 100,000 g's shock, providing high reliability.

The IC amplifier operates from constant current type power units (many types are available from Dytran) and may be supplied with from 2 to 20 mA of current, depending upon the length of cable being driven by the sensor. The current is supplied to the source terminal of the sensor amplifier (see Fig. 2) and this point is normally biased at approximately +10 Volts DC.
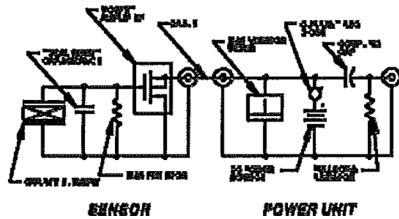
**Figure 2 System Schematic**

The DC bias voltage of the sensor amplifier is blocked by the 10 uF coupling capacitor in the power unit and only the dynamic signal from the sensor is allowed to pass to the readout instrument.

Referring to Fig. 2, within the accelerometer, the resistor from the gate of the MOSFET to ground serves to bias the amplifier at its proper operating point and it also establishes the low frequency response of the sensor by setting the discharge time constant (TC) of the accelerometer. This resistor and the total shunt capacitance C across it (the crystal, gate and stray capacitance) set the TC which in turn sets the low frequency response as follows:

$$f_{-3db} = \frac{.16}{RC} \quad \text{(Eq. 1)}$$

where:

$f_{-3db}$ = The lower -3db frequency (Hz)

R = bias resistor value     (Ohms)

C = total shunt capacitance across bias resistor

The product RC is also known as discharge Time Constant or TC. Series 3019A has a TC of .5 seconds. Applying equation 1, the lower -3db frequency of Series 3019A is .32 Hz and the -5% frequency is 3 times the -3db frequency or .96 Hz.

Referring to Fig. 2, most Dytran power units feature a DC voltmeter which reads this bias voltage from the sensor and as such, serves as a very useful system trouble shooting tool. (For more information on this feature, refer to the

paper "Low Impedance Voltage Mode (LIVM) Theory and Operation", included with this manual.

Dytran offers many types of current source power units to operate LIVM sensors like Series 3019A. These include the single channel battery operated Models 4102 and 4105, which supply fixed 2 mA of constant current, the line powered single channel model 4110, and the four channel model 4114, both of which feature adjustable drive current. Also included are many types of other multiple channel units with 6, 12 and 16 sensor channels.

**INSTALLATION**

Refer to Outline/Installation drawing 127-3019A or drawing 127-3019A1 for this section.

To install either Model, it is necessary to select or prepare a smooth, flat mounting area at least .375 in diameter. The surface should be flat to .001 TIR and may be prepared by various machining methods such as spotfacing, grinding, turning, etc. if required.

It is important that the accelerometer base be in intimate contact with the mounting surface for best high frequency response and for faithful reproduction of the calibrated sensitivity over all frequencies.

For Model 3019A, at the center of the selected mounting area, drill and tap a 1/4-28, UNF-2B mounting hole with minimum thread depth of .250. (Be careful to ensure that the drilled hole is perpendicular to the mounting surface to within ±1°.) For Model 3019A1, drill and tap a 10-32 UNF-2b mounting hole with a minimum thread depth of .250.

After this operation, clean the area thoroughly to remove all traces of oil, machining chips and burrs which could preclude intimate contact between mounting surfaces.

Coat one of the mating surfaces with a thin layer of silicone grease, then thread the Series 3019A or A1 integral stud into the mounting hole so that the mounting surfaces just meet. Inspect the mating surfaces to see that they contact squarely, inspecting for chips which may have become lodged between the mating surfaces. If the contact looks square, proceed to torque the sensor down with 20 to 25 lb-inches of torque, preferably using a torque wrench with a 3/8 in. deep socket gripping on the 3/8 in. hex of the case.

Connect the accelerometer to the power unit using Model 6010AXX or 6011AXX coaxial cable. Model 6010A is used when the power unit

has 10-32 input connectors and Model 6011A is used when the power unit has BNC jack input connectors. Carefully tighten the 10-32 knurled nut at the sensor, by hand to ensure a secure connection. Do not use pliers on this cable nut as this may damage the cable or sensor connector.

Under high shock or high vibration conditions, it may be discovered that the cable nut has become loose and is causing erratic readings. Under these conditions, it may be advisable to use a mild thread locking agent such as Loctite® on the threads of the 10-32 connector when re-installing the cable.

Connect the "Output" jack of the power unit to the readout instrument (oscilloscope, recorder, meter, etc.) and proceed with the measurement.

## MONITOR METER

Refer to the section "Monitor Meter" in the paper, "Low Impedance Voltage Mode (LIVM) Theory and Operation", supplied with this manual for a guide to using the monitor meter on the front of most Dytran power units as a handy trouble shooting tool for LIVM systems.

## MAINTENANCE AND REPAIR

The sealed construction of the 3019A Series precludes most maintenance other than that necessary to maintain a smooth mounting surface at the accelerometer base mounting surface.

Periodically inspect the mounting base surface for nicks or deep scratches, gouges and other imperfections which could prevent intimate contact between mating surfaces. If surface imperfections are discovered, you may want to consider returning the unit to the factory for a dressing of the mounting surface.

The electrical connector may be cleaned if necessary, with a cloth or paper wipe dipped in Freon ® or alcohol. After this operation, it may be beneficial to bake the sensor out in a drying oven at 200 to 250 °F for an hour or so. **Never higher than +300°F!**

Should a problem arise with the sensor, contact the factory for assistance. If the instrument must be returned for evaluation, you will be issued a **Returned Material Authorization (RMA)** number to help guide the instrument through the evaluation process. Please do not return any instrument or power unit to the factory without first obtaining an RMA number.

We will not proceed with repairs without first notifying you of charges (if any) and obtaining your approval. There is no charge for evaluation of the instrument.

## CAUTIONS

1) Do not store or use Series 3019A above +300°F.

2) For best frequency response, measure the mounting torque, don't guess.

3) Never connect the sensor to a power source (battery or power supply) which does nor have current limiting, 20 mA MAX! This will immediately destroy the integral IC amplifier.

4) Do not attempt to measure the resistance at the sensor connector as many ohmmeters supply too much current for the internal IC and may destroy it.

| REV | ECN | DESCRIPTION | BY/DATE | CHK | APPR |
|---|---|---|---|---|---|
| A | 10476 | REMOVED WELD GROOVES | NC/11-5-13 | | |

.375 HEX

Ø .409 HEX CORNERS

ARROW INDICATES SENSE AND DIRECTION OF ACCELERATION FOR POSITIVE - GOING OUTPUT SIGNAL

10-32 COAXIAL CONNECTOR

ELECTRICAL ISOLATION, BASE TO CASE, 10 MEGOHMS, MIN

1/4-28 UNF-2A MOUNTING STUD

Ø.36

.73

.20

Ø .360

**MOUNTING PORT PREPARATION:**
PREPARE FLAT SURFACE OF AT LEAST .360 DIA. WITH A FINISH OF  ᴺ/  OR BETTER AND FLAT TO .001 TIR.
AT CENTER OF FLAT AREA:
DRILL Ø .213 X .35 DEEP MIN.
TAP 1/4-28 UNF-2B X .25 MIN DEPTH
HOLE TO BE PERPENDICULAR WITHIN ±1°

3. MATERIAL: 300 SERIES STAINLESS STEEL.

2. WEIGHT: 8 GRAMS.

1. RECOMMENDED MOUNTING TORQUE ON 3/8 IN. HEX: 20 TO 25 LB.-INCHES.

DYTRAN INSTRUMENTS, INC.
MASTER
ONLY IF IN RED
CHATSWORTH, CA.

| SCALE 2X | DESIGN N.C. | DATE 6/2/98 | PART NO. | MODEL 3019A | | REV A |
|---|---|---|---|---|---|---|
| DRAWN N.C. | | DATE 6/2/98 | MATL. | | | |
| CHECKED R.A. | | DATE 6/2/98 | NEXT ASSEMBLY | | USED ON | |
| APPROVED | | | | | | |

TITLE
OUTLINE/INSTALLATION DRAWING, HIGH FREQUENCY ACCELEROMETER MODEL 3019A

DWG NO. 127-**3019A**

SHEET 1 OF 1

## LOW IMPEDANCE VOLTAGE MODE (LIVM) SYSTEMS, THEORY AND OPERATION

### LIVM: WHAT IS IT?

LIVM is Dytran's trademark for our version of Low Impedance Voltage Mode piezoelectric instruments, i.e., piezo instruments with integral-impedance-converting amplifiers operating from constant current supplies over two wires. LIVM instruments are entirely compatible the new industry standard IEPE designated systems.

LIVM instruments produced at Dytran include force, pressure and acceleration sensors. Each class of sensors is produced in many varieties for a wide range of applications.

Also falling under the class of LIVM instruments are in-line charge amplifiers that utilize the same two-wire constant current operating mode as the LIVM sensors.

Operating principles for LIVM sensors and in-line amplifiers are similar in that they utilize the same two-wire constant current operating mode. The amplifiers built into the sensors are either MOSFET-input voltage or charge amplifiers or JFET-input charge amplifiers.

All types of LIVM amplifiers serve to convert the very high impedance of the piezoelectric crystals to much lower impedance voltage signals that have the capability of driving long cables with little or no signal degradation.
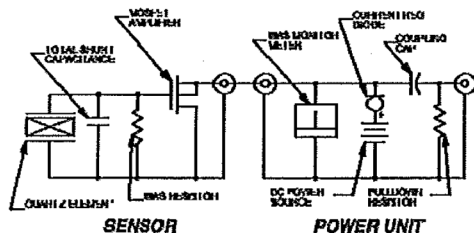
### THEORY OF OPERATION



**FIGURE 1: TYPICAL LIVM VOLTAGE MODE SYSTEM**

Figure 1 is a simplified schematic of a basic LIVM system including the sensor with integral electronics, the cable and the power unit. The sensor amplifier in this case is the unity gain voltage follower. This is the type of amplifier used in most LIVM sensors and almost exclusively used with quartz element sensors.

The sensing element (force, pressure or acceleration), usually made with quartz or piezoceramic crystals, is connected directly to the gate of a FET input integrated circuit (IC) amplifier. This amplifier is operated as a source follower and, as such, has unity voltage gain.

The source terminal of the IC is supplied with constant current over the range of 2 to 20 mA at a compliance (supply) voltage of +18 to +30 volts DC. The power unit may take the form of many different configurations from simple battery powered 2 mA units with constant current diode, to line-powered adjustable current power units able to supply 2 to 20 mA of constant current from adjustable constant current circuits.

In either case, the constant current device (current diode or constant current circuit), acts as the source impedance for the unity gain IC built into the sensor or for the in-line charge amplifier.

Under quiescent conditions, the IC will bias itself at approximately +10 volts DC at the input (source) terminal of the sensor. (Some special variations will bias at different voltages depending upon the specific application). This sensor bias voltage is monitored and displayed, on most Dytran power units, and this feature serves as a handy trouble-shooting tool, serving as an indicator for normal or abnormal operation. (More on this topic in a following section, "The fault monitoring monitor as a trouble-shooting tool").

The sensor signal, produced by the measurand acting upon the piezo element, is superimposed upon the sensor bias voltage and appears at the "Sensor" jack of the power unit. At this point, the DC bias portion of the signal is blocked by a coupling capacitor and the AC (signal) portion is coupled directly to the "Output" jack of the power unit.

The Output jack may then be connected directly to the input of readout instruments (oscilloscopes, spectrum analyzers, AC meters, frequency counters, etc.). The very low output impedance of the LIVM sensor (about 150 Ohms) makes the effect of most readout instruments on the signal, negligible.

Be aware that the coupling capacitor in the power unit (usually 10 μF) and the impedance of the readout load constitute a high-pass filter that may set the low frequency response of the system below the LF response built into the sensor. In most accelerometer applications, the 10 μF capacitor provides ample time constant to allow vibration measurements down to fractions of a Hz.

Dytran also manufactures DC-coupled power unit for LIVM sensors that utilizes an active variable voltage level amplifier circuit to "buck out" the DC bias voltage of the sensor. One such unit, model 4115B, supplies constant current to the sensor and direct-couples the sensor to the output jack eliminating the coupling capacitor. This feature allows the user to take full advantage of the long time constant built into the sensor and precludes the effect of readout instrument load on the low frequency response of the system. Model 4115B is especially useful for very long-duration (quasi-static) measurements especially with force and pressure sensors.

### OPERATION, GENERAL

**Special note:** LIVM sensors depend on the power unit to supply a fixed amount of current to the sensor IC. These IC circuits will absorb any amount of current supplied until they exceed their power rating and burn up. For this reason, never apply power to an LIVM sensor without this current limiting protection. This precludes the connection of LIVM sensors directly to batteries, DC power units and many types of resistance measuring devices. Never measure the continuity of an LIVM sensor with any type of Ohmmeter. This type of measurement is redundant and may lead to destruction of the sensor. To determine if the IC is intact, use the monitor meter on the front panel of your Dytran power unit. This topic is covered in the following section, "The fault monitoring meter as a trouble-shooting tool".

1

After installing the sensor in accordance with instructions in the operating guide (manual) supplied with each sensor, connect the sensor to the power unit's "Sensor" jack. This jack, in most cases, is a BNC coaxial connector. You should have been supplied with the proper cable to connect the sensor to the power unit you have selected. If you were not and/or do not have such a cable, contact the factory for help.

It is important to carefully support the sensor cable, especially in situations where there is movement between the sensor and its surroundings. This practice will prolong cable life and will diminish or preclude the effects of triboelectric (cable generated) noise on the signal.

## THE FAULT-MONITOR METER: A TROUBLE -SHOOTING TOOL

Most Dytran power units incorporate a dc voltmeter on the front panel that measures the DC bias voltage at the sensor terminal. Measuring this voltage supplies information about the "health" of the measurement system. The three conditions it can identify are 1) normal operation, 2) shorted cable or sensor or faulty power unit and 3) open sensor or cable connection. We will examine each possibility here.

NOTE: The fault-monitor meter may be the LED style shown on the left, Fig. 2, or the D'Arsonval panel meter style shown on the right, Fig. 2.
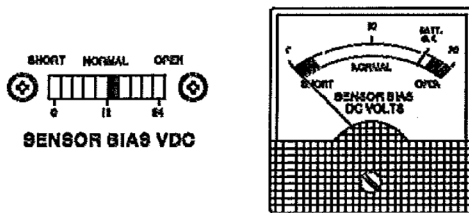


## FIGURE 2: TYPICAL FAULT MONITOR METERS

## NORMAL OPERATION

Under most normal operating conditions, the monitor meter will indicate approx. mid-scale (+10 to +13 volts DC) when the sensor is connected. Many of the meter faces have a "Normal" area delineated to indicate that the sensor is functioning and the cable from sensor to power unit is neither open nor shorted. It is possible that certain failure modes of the sensor can produce "Normal" indications but these modes are very rare. In most cases, if the meter reads in the "Normal" area, the system is viable.

As a further quick check on normal operation, with some sensors such as pressure and force sensors, pressing on the diaphragm or force sensitive surface with a finger can cause the monitor meter pointer to deflect showing that the sensor is "alive". With some higher sensitivity accelerometers, shaking them by hand can deflect the monitor meter enough to show the sensor is functioning.

## OPEN SENSOR OR CABLE (FULL SCALE METER READING)

If the sensor amplifier is blown or the cable connecting sensor to power unit is open, the monitor meter will read in the "OPEN" area of the scale since the current source in the power unit has no load. To check if the problem is in the sensor, disconnect the sensor from its cable (leaving the other end connected to the power unit), and short across the open end of the cable with a metallic object while observing the meter. If the meter does not indicate zero ("short") while the sensor end of the cable is shorted, the cable is open. Replace the cable and try the sensor again, looking for the "Normal" indication.

If the meter reads zero when the short is applied, the cable is OK but the sensor is open. If another sensor is available, try it to verify the finding.

## SHORTED SENSOR OR CABLE ("SHORT" METER READING)

If the fault-monitor meter reads in the "Short" area after connecting the sensor, this means that there is a short in the cable or sensor.

This condition cannot damage the power unit since the constant current circuit in the power unit limits the maximum current. Sometimes, shards of metal can scrape off of the cable connector of the 10-32 cables and these may short across the sensor connection. Check for this. Cleaning with a stiff-bristled brush will dislodge such metal shards.

If a short is still indicated, then the problem is with the cable or the power unit. Disconnect the cable from the power unit and observe the meter reading. If the meter reads full scale, the power unit is OK and the problem is a shorted cable or sensor. Replace the cable to verify.

## MAINTENANCE AND REPAIR

Because of their small size and sealed construction, field maintenance of **LIVM** sensors is limited to cleaning of connectors and maintenance of mounting surfaces.

Clean connectors with a cloth or paper wipe dipped in solvents such as alcohol, Freon, etc. For hermetically sealed units, acetone may be used also. Acetone is not recommended for non-hermetic units.

Clean epoxy from the mounting surfaces of accelerometers, if necessary, with acetone or other solvents to dissolve and remove epoxies and other adhesives.

If the problem you are having is poor low frequency response and the sensor is not hermetically sealed, baking in a 250° oven for one hour will often get rid of moisture that may have condensed and shorted across the crystals which would shortened the discharge time constant.

If you cannot solve the problem, call the factory for assistance in trouble-shooting the system or for instructions for returning the instrument for evaluation and/or possible repair.

If the instrument is to be returned, you will be issued a Returned Material Authorization (RMA) number by the service department to help speed the instrument through the evaluation process. Do not return an instrument without first contacting the factory.

2

**UNHOLTZ-DICKIE CORPORATION**
Vibration Test Equipment

- trusted supplier since 1959

## S-Series Electrodynamic Shaker Systems

The S-Series Vibration Test Systems cover a wide range of force output (100 lbf to 8,500 lbf) in support of small to moderately large payloads. The S-Series shakers are supplied with SA, SAI or TA Series power amplifiers. These systems support a variety of applications including product development and design conformance, product qualification and certification, accelerated life testing and environmental stress screening. The S-Series also includes the industry's highest shock system capable of 1500 g peak. Overall, the S-Series provides exceptional performance and proven reliability in hundreds of installations around the world. Installation is simple, requiring standard electrical connections, foundation support and blower mounting. Standard system configurations are tabulated below. Custom systems can be discussed with applications engineers.

### Shaker Model: S452

Force Range: 4,500 to 6,000 lbs (20 to 26,7 kN)

Armature Sizes: 13.3 inch (337 mm), 17.5 inch (445 mm)

### Features

4,500 to 6,000 lbs (20 to 26.7 kN) Force

Armature Weight with Inserts 50 lbs (22.7 kg)

200 g Shock

2 inch (51 mm) Displacement

600 lbs (272 kg) Internal Pneumatic Load Support

13.3 inch (337 mm) Diameter Armature, 12 inch (305 mm) Outer Bolt Hole Circle

**NEW 17.5 inch (445 mm) Armature now available!**

Three Base Configurations:
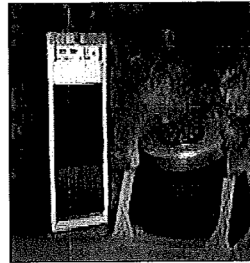
Low Profile (LP)

Pedestal Base (PB)

ST Series Slip Table Assembly (ST)

Completely Air Cooled

Modular, High Efficiency Class-D SA or SAI Series Power Amplifier

Combined Environment Support

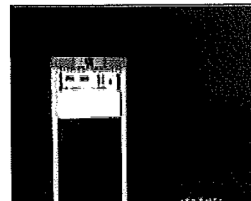SA-Command Link APEX SL / Amplifier Remote Interface

### Shaker Model: S202

Force Range: 1,000 to 2,200 lbs (4.4 to 9.8 kN)

Armature Size: 13.3 inch (337 mm)

### Features

1,000 to 2,200 lbs (4.4 to 9.8 kN) Force

http://www.udco.com/sseries.shtml                                    5/13/2014